



Universidad
del País Vasco

Euskal Herriko
Unibertsitatea

FACULTY
OF ENGINEERING
BILBAO
UNIVERSITY
OF THE BASQUE
COUNTRY



**ADVANCED CATALYTIC AND PHOTOCATALYTIC
TECHNOLOGIES FOR METHANE GENERATION FROM
RENEWABLE ENERGIES**

PhD Thesis

Rafael Canales Larrazabal

Thesis Advisor

Prof. Victoria Laura Barrio

(c) 2024 RAFAEL CANALES LARRAZABAL

**ADVANCED CATALYTIC AND PHOTOCATALYTIC TECHNOLOGIES
FOR METHANE GENERATION FROM RENEWABLE ENERGIES**

*A memory submitted to the University of the Basque Country in fulfilment of the requirements for the degree of PhD presented by **Rafael Canales Larrazabal***

Thesis Advisor: **Prof. Victoria Laura Barrio**

Bilbao, 2023

Resumen

La presente tesis doctoral se inició en octubre de 2018 con el apoyo del Ministerio de Economía, Industria y Competitividad en el marco del proyecto TECNORENO (Tecnologías catalíticas y fotocatalíticas avanzadas para la generación de metano a partir de energías renovables; ENE2017-82250-R) y el grupo de investigación SUPREN- el cual forma parte del Departamento de Ingeniería Química y Medio Ambiente de la Escuela de Ingeniería de Bilbao dentro de la Universidad del País Vasco (UPV/EHU). Este trabajo ha continuado con el proyecto HYVALUE (Desarrollos innovadores en la cadena de valor del hidrógeno: desde la generación de electricidad con fuentes renovables hasta su uso; PID2020-112889RB-I0) y se ha realizado bajo la supervisión de la Dra. Victoria Laura Barrio Cagigal y el Dr. José Francisco Cambra Ibañez. Tal y como se detalla, en la memoria científico-técnica y para la mención de doctorado internacional, durante la tesis se realizó una estancia de investigación de 4 meses en el *Istituto di Tecnologie Avanzate per l'Energia (CNR-ITAE)* de Messina (Italia) bajo la supervisión del Dr. Antonio Vita y del director Dr. Antonino Salvatore Arico y con el amable apoyo del Dr. Giovanni Drago Ferrante y la Dr. Cristina Italiano.

Durante estos años de trabajo realizado, se han desarrollado nuevos sistemas catalíticos para la mejora y optimización de la reacción de Sabatier para la producción principalmente de metano de origen renovable a partir de dióxido de carbono e hidrógeno, a través de dos tipos de proceso diferentes: catalítico y fotocatalítico. Siendo esta último, un proceso novedoso en cuanto a la metodología y uso de equipos nuevos y que anteriormente no se poseían conocimientos de su posible repercusión. Se observó una mejora respecto a la actividad durante el empleo de las dos fuentes de

luz LED (ultravioleta y visible). Respecto a la presente tesis, esta se engloba en seis capítulos que se describen a continuación.

El **Capítulo I**, trata de la situación actual del uso de las energías renovables y las proyecciones a futuro de mayores implementaciones. A su vez, debido a la necesidad de mitigación de las emisiones de CO₂, uno de sus vectores energéticos es su aprovechamiento como reactivo para la producción de metano, siendo este último un producto de alto interés añadido y su relación con los SDGs.

El **Capítulo II**, analiza las tecnologías actuales para la generación de metano, siendo el *Power-to-Gas* la que concierne a dicha tesis doctoral. Se trata de un proyecto con alta repercusión europea y que además se encuentra actualmente extendiéndose globalmente. Se analizan a su vez, tecnologías actuales para la producción de hidrógeno como la introducción de sistemas de captura de dióxido de carbono para poder incorporar ambos gases en nuestro proceso de producción de metano. Al metano se le considera como un producto energético con demanda industrial y doméstica, y a su vez con infraestructuras adecuadas y conocidas para su transporte y distribución. Además, existe un alto interés en poder implementar en un futuro los diferentes estudios en relación a los desarrollados por el grupo SuPrEn, ya que las tecnologías que se están analizando hasta la fecha de la tesis, podrían complementarse y así poder optimizar globalmente el presente documento y dar un uso alternativo y con mayor interés como conjunto.

El **Capítulo III** define el objetivo de la presente tesis. Desde el comienzo de los materiales presentados en la memoria científico-técnica, así como los propuestos a posteriori de la misma y que gracias a los resultados obtenidos se publicaron tres artículos, uno en la revista científica Heliyon bajo el título: *Ni–Co bimetallic and monometallic hydrotalcite-like materials for enhanced CO₂ methanation in Sabatier reaction*, con autores: Rafael Canales, Miryam Gil-Calvo y V. Laura Barrio (DOI: <https://doi.org/10.1016/j.heliyon.2023.e18456>). Un segundo, en la revista MDPI materials, bajo el título: *Photo- and Thermocatalytic CO₂ Methanation: A Comparison of Ni/Al₂O₃ and Ni–Ce Hydrotalcite-Derived Materials under UV and Visible Light*, con autores: Rafael Canales y V. Laura Barrio (DOI: <https://doi.org/10.3390/ma16175907>). Por último, un tercero titulado: *Ni–Fe nanoparticles prepared using hydrotalcite precursors enhance the photocatalytic performance of CO₂ methanation*, con autores: Rafael Canales, Ion Agirre y V. Laura Barrio en la revista International Journal of Hydrogen Energy, que se encuentra aceptado desde el 10 de diciembre de 2023.

El **Capítulo IV** trata de los métodos de preparación experimentales de todos los catalizadores sintetizados y la caracterización necesaria para el completo conocimiento del comportamiento previo y posterior a los ensayos. Respecto a los sistemas Ni/Al₂O₃ y Ni/TiO₂ previamente estudiados en el grupo SuPrEn, la carga de Ni metálico se optimizó, siendo un 25% el óptimo, ya que obtuvo los mejores resultados catalíticos. La síntesis se llevó a cabo utilizando varios materiales derivados de una hidrotalcita con diferentes cargas metálicas y promotores de Fe, Ce, Ni y Co. Finalmente, las hidrotalcitas optimizadas y, especialmente, para el catalizador comercial Katalco, se

realizaron estudios de caracterización y síntesis para su posible escalado a nivel industrial impregnados en diferentes soportes estructurados, así como finalmente comparar la mejora catalítica respecto a las condiciones realizadas en el laboratorio.

Capítulo V, se procedieron a analizar experimentalmente los catalizadores para la reacción de metanización de CO₂ bajo tres condiciones diferentes: i) Catalítica sin luz, ii) Fotocatalítica con luz LED de 365 nm y iii) Fotocatalítica con luz LED de 470 nm. Los resultados correspondientes a este capítulo con relación a los materiales modificados: hidrotalcitas de ceria, cobalto y hierro respecto a sistemas mono-metálicos, fueron publicados en las revistas mencionadas anteriormente. Las hidrotalcitas mencionadas, mejoraron sustancialmente, los resultados respecto a los materiales monometálicos debido al uso de agentes promotores. Se observó como la mayor basicidad del material ofrecido principalmente por el óxido de magnesio junto con el uso del promotor que presenta vacantes de oxígeno como la ceria, mejoraron no solo los resultados respecto a los convencionales, sino que se obtuvieron datos muy positivos y que pueden ofrecer un alto interés para su uso industrial con el uso del espectro solar como fuente energética.

Finalmente, se analizaron los comportamientos de adhesión, espesor y actividad de dos catalizadores impregnados en diferentes espumas de alúmina durante la estancia en Italia. Los resultados obtenidos mejoraron respecto a los ensayados previamente en cuanto a transferencia de materia y energía se refieren (para una alúmina de 30 PPI, *pores per inch*, con una densidad de 0.1 g/cm³). No se precisaron, por tanto, elementos

homogeneizadores de temperatura debido a la mejora de gradientes térmicos dentro del sistema de reacción catalítica y a su vez, mejoraron la caída de presión. Se aumenta, además, su superficie de contacto activa y una mejor resistencia mecánica para resistir las condiciones de operación adversas como son presiones y altas temperaturas.

El **Capítulo VI** comprende las conclusiones finales, las cuales se derivan del análisis de todos los datos obtenidos y se catalogan las propiedades necesarias para que estudios posteriores se basen en estas premisas. Se proporciona una visión más clara sobre el uso de sistemas fotocatalíticos y cómo han mejorado en comparación con los sistemas termocatalíticos. Cabe destacar que, la presencia de centros básicos débiles y/o moderados debido a su importante papel en la producción de metano, sobre todo a bajas temperaturas (473-523 K). El uso de materiales que proporcionen vacantes de oxígeno, como es el caso de la ceria, y el uso de materiales estructurados, son dos potenciales mejoras que pueden permitir el escalado para pasar de materiales probados en laboratorio a aplicaciones industriales.

Abstract

The present doctoral thesis was initiated in October 2018 with the support of the Ministry of Economy, Industry, and Competitiveness within the framework of the TECNORENO project entitled: *Advanced Catalytic and Photocatalytic Technologies for Methane Generation from Renewable Energies* (ref.: ENE2017-82250-R) and the SUPREN- *SUstainable PRocess ENgineering* research group, which is part of the Department of Chemical and Environmental Engineering at the Bilbao School of Engineering, University of the Basque Country (UPV/EHU). This research work has continued with the HYVALUE project entitled: *Innovative Developments in the Hydrogen Value Chain: from Renewable Electricity Generation to Utilization* (PID2020-112889RB-I0) and has been carried out under the supervision of Prof. Victoria Laura Barrio Cagigal. As detailed in the scientific-technical report and for international doctoral recognition, a 4-month research stay was conducted at the prestigious *Istituto di Tecnologie Avanzate per l'Energia (CNR-ITAE)* in Messina, Italy, under the supervision of Dr. Antonio Vita and Director Dr. Antonino Salvatore Arico, with the kind support of Dr. Giovanni Drago Ferrante and Dr. Cristina Italiano.

Throughout all these years working, new catalytic systems have been developed to enhance and optimize the Sabatier reaction for the production of renewable methane from carbon dioxide and hydrogen, through thermocatalytic and photocatalytic processes. The latter, being a novel process in terms of methodology and the use of new equipment with previously unknown potential repercussions. Activity improved using LED lights (UV and vis). This research work is organized into six chapters.

Chapter I which addresses the current situation of renewable energy use, projections and future implementations. Additionally, due to the need to mitigate CO₂ emissions, one of the energy vectors is its utilization as a reactant for methane production, with the latter being a product of high-added interest and its relation to the SDGs. Different efforts and strategies have been implemented to reduce CO₂ emissions, global warming and climate change.

Chapter II analyzes current technologies for methane generation, with a focus on Power-to-Gas, which is relevant to this doctoral thesis, especially, for the Power-to-Methane. This process typically includes two main steps: water electrolysis to produce hydrogen, and then the Sabatier Process where hydrogen is combined with CO₂ to produce CH₄. Current technologies for hydrogen production are also examined to incorporate this gas into the methane production process and also it is demonstrated how the photocatalytic effect induced by light, positively impacts into the previously cited results.

Chapter III defines the objective of the present thesis. The synthesized materials are presented, as well as the characterization conducted before and after their use in various experiments, and finally, their implementation in the photocatalytic activity plant. These analyses led to three relevant publications in topic-relevant indexed journals (detailed in PhD candidate curricula).

Chapter IV deals with the experimental preparation methods of all synthesized catalysts and the necessary characterization for a complete understanding of their behavior before and after the experiments. Regarding the Ni/Al₂O₃ and Ni/TiO₂ materials previously analyzed in the SuPrEn group, the metallic Ni loading was optimized to 25%, as it obtained the best catalytic results. Synthesis were conducted using various hydrotalcite derived materials with different metallic loadings and various promoters such as Fe, Ce, Ni, and Co. Finally, optimized hydrotalcites and a commercial catalyst were dedicated to structured catalysts development as a potential materials scale-up for methane production.

Chapter V involves the experimental analysis of catalysts for the CO₂ methanation reaction under three different conditions: I) Catalysis without light, II) Photocatalysis with 365 nm LED light, and III) Photocatalysis with 470 nm LED light. The materials can be summarized in terms of their activity and selectivity towards methane as follows: hydrotalcites > Ni/Al₂O₃ > Ni/TiO₂ > Au/TiO₂. Regarding the use of different promoters in hydrotalcites, ceria yielded the best results with activity at very low temperature. Finally, the adhesion behavior and thickness of two catalysts impregnated in different alumina foams were analyzed. The best results in terms of adhesion, improvement in thermal gradient and drop pressure during activity tests were obtained with a 30 PPI (pores per inch) alumina open-cell foam with a density of 0.1 g/cm³.

Chapter VI consists of the conclusions after analyzing all the obtained data, and the necessary properties for subsequent studies based on these premises are categorized.

Photocatalytic processes are studied and improvement has been demonstrated if compared with thermocatalytic processes. Emphasis is placed on the importance of weak to moderate basic centers due to their critical role in the methane production temperature (473-523 K). The use of materials that provide oxygen vacancies, such as ceria, and the utilization of structured materials are considered as two potential developments for process scaling up from laboratory-tested materials to industrial applications.

INDEX

CHAPTER I. INTRODUCTION.....	3
I.1. Renewable energy: Current situation in Europe and worldwide	3
I.2. Green methane: a renewable energy vector	6
I.3. Sustainable Development Goals (SDGs) Fund.....	9
CHAPTER II. STATE OF ART	17
II.1. CH ₄ production directly from biogas	17
II.2. Power-to-Gas (PtG).....	18
II.2.1. Hydrogen production via water electrolysis.....	20
II.2.2. CO ₂ removal from air	24
II.2.3. CO ₂ Methanation.....	26
II.3. Power-to-Liquids (PtL).....	28
II.4. Reactors for Sabatier process.....	29
II.4.1. Fixed bed reactor	29
II.4.2. Fluidized bed reactor	31
II.4.3. Three phase reactor	32
II.4.4. Photocatalytic reactor	33
II.5. Critical raw materials	36
II.6. Sabatier reaction catalysts	39
II.6.1. Noble and non-noble metal catalyst	39

II.6.2. Supports.....	40
II.6.3. Hydrotalcites	40
II.7. Structured catalysts supported on foams	41
II.8. Summary of current the catalytic and photocatalytic catalysts	42
CHAPTER III. OBJECTIVES	59
CHAPTER IV. EXPERIMENTAL	65
IV.1. Catalyst Preparation.....	65
IV.2. Catalyst characterization for monometallic and HTC materials	70
IV.2.1. N ₂ Adsorption-Desorption Isotherms.....	70
IV.2.2. ICP-OES.....	70
IV.2.3. H ₂ -TPR	71
IV.2.4. CO ₂ -TPD.....	71
IV.2.5. XRD	72
IV.2.6. UV-Vis-DRS	72
IV.2.7. XPS	72
IV.2.8. H ₂ -Chemisorption.....	73
IV.2.9. STEM-EDS.....	73
IV.3. Wash-coating for CO ₂ methanation.....	73
IV.3.1. Catalyst preparation	73
IV.3.2. Catalyst characterization for wash-coating process	77

IV.4. Activity test for CO ₂ methanation (Photo and Fixed bed reactor)	78
IV.4.1. Photo-reactor	78
IV.4.2. Fixed-bed reactor	80
CHAPTER V. RESULTS AND DISCUSSION.....	89
V.1. Monometallic Ni/Al ₂ O ₃ , Ni/TiO ₂ & Au/TiO ₂	89
V.1.1. Structural properties of the calcined catalysts	89
V.1.2. Reducibility of the catalysts	90
V.1.3. CO ₂ -TPD	90
V.1.4. UV-Vis DRS.....	92
V.1.5. H ₂ -Chemisorption.....	93
V.1.6. STEM-EDS.....	93
V.1.7. Activity results.....	94
V.2. Hydrotalcite derived materials compared with monometallic catalysts	95
V.2.1. Cerium promoter.....	95
V.2.1.1. Structural properties of the calcined catalysts and ICP-OES	95
V.2.1.2. The Programmed Reduction Temperature of H ₂	96
V.2.1.3. CO ₂ -TPD	98
V.2.1.4. XRD.....	99
V.2.1.5. H ₂ Chemisorption.....	101
V.2.1.6. XPS.....	102
V.2.1.7. UV-vis-NIR DRS and Band Gap	105
V.2.1.8. Performance of the catalysts.....	107
V.2.1.9. STEM-EDS and XPS of the Used Catalysts	111

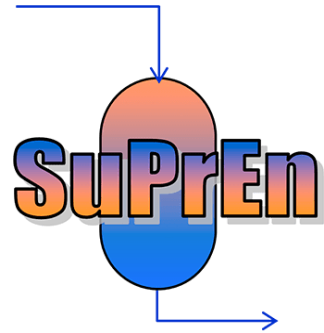
V.2.2. Cobalt promoter	114
V.2.2.1. Chemical and textural properties	114
V.2.2.2. XRD	114
V.2.2.3. H ₂ -Temperature Programmed Reduction	116
V.2.2.4. CO ₂ -Temperature Programmed Desorption	117
V.2.2.5. UV-vis DRS.....	119
V.2.2.6. XPS.....	120
V.2.2.7. STEM-EDS	122
V.2.2.8. Catalyst performance	122
V.2.3. Iron promoter	126
V.2.3.1. Textural properties	126
V.2.3.2. Crystalline phases	127
V.2.3.3. Samples reducibility	129
V.2.3.4. XPS.....	130
V.2.3.5. UV-vis DRS.....	132
V.2.3.6. CO ₂ -TPD analysis	133
V.2.3.7. STEM-EDS	135
V.2.3.8. CO ₂ methanation results of activity and stability test	137
V.2.4. Molybdenum promoter	142
V.2.4.1. Textural properties and metal composition	142
V.2.4.1. Reducibility and basic sites.....	142
V.2.4.1. Activity results	143
V.3. Washcoating of Katalco and Ce-hydrotalcite catalyst on open cell alumina foams	145
V.3.1. Influence of speed velocity on spin coating	145
V.3.2. Influence of the variation of catalyst loading on the open cell foams	148
V.3.3. Influence of the geometry and porosity of the open cell foams	149

V.3.4. Effect of processing conditions	151
V.3.5. Estimation of average thickness by mathematic equations	153
V.3.6. CO ₂ methanation activity results on commercial Katalco catalyst wash-coated on different alumina open cell foams	157
CHAPTER VI. CONCLUSIONS	177
INDEX OF FIGURES AND TABLES	181



CHAPTER I

INTRODUCTION



Rafael Canales
Larrazabal
Bilbao, 2023



Universidad
del País Vasco

Euskal Herriko
Unibertsitatea

MDe

Master eta Doktorego Eskola
Escuela de Máster y Doctorado
Master and Doctoral School

CHAPTER I. INTRODUCTION

I.1. Renewable energy: Current situation in Europe and worldwide

Climate change is a serious concern for worldwide. The impact of global warming is experienced and its consequences such as: extreme heat in Europe, the temperatures above the Artic Circle were 5 °C higher than usual and flood events particularly affecting Central and Eastern Europe in the recent years, are some of the effect associated to this global warming.

Without stepping forward to face the climate change, an increase of 2 °C turning the Earth into a “hothouse” and irreversible climate impact.

In addition, there is an increase in energy consumption associated with overpopulation leading to higher global CO₂ emissions. This growth will radically transform our energy vector, modernizing the industrial systems and cities which will require maximizing the perks from energy efficiency, the deployment of renewable technology and the use of this electricity to fully decarbonize energy source of sectors such as heating, transport and industry and thus, reduce greenhouse gas emissions [1]. *Figure I-1* shows the overall supply of energy for all activities concerning Europe, excluding international maritime bunkers and the different scenarios set by 2050.

In terms of global CO₂ emissions from energy combustion and industrial process estimated region-by-region and fuel-by-fuel analysis, grew 0.9% or 321 Mt in 2022

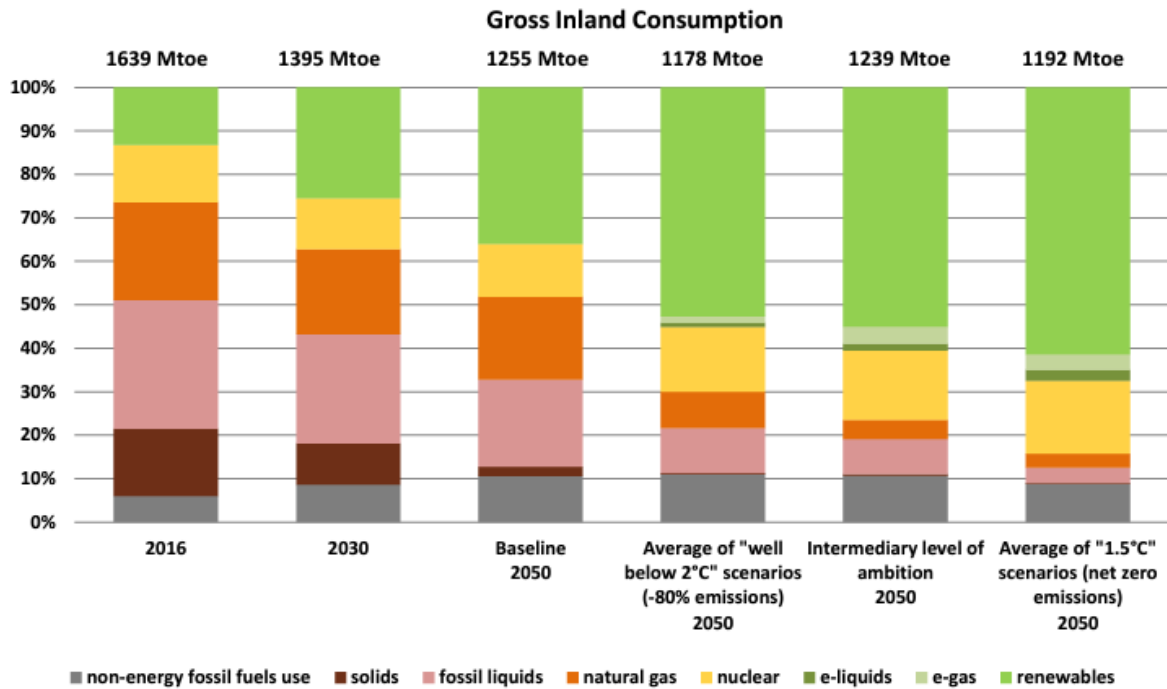


Figure I-1. Fuel mix in Gross Inland Consumption in Europe

reaching the maximum emission of 36.8 Gt as shown in *Figure I-1*. Solar PV and wind generation were used to avoid around 465 Mt CO₂ in power sector emissions and 85 Mt CO₂ from other renewable resources, electric vehicles and heat pumps [2].

From 2022 to 2027, renewables are expected to grow by almost 2400 GW. Solar PV has been the fastest growing technology (150 GW added in 2021) followed by the wind energy, which installations need to be double from 2021. On Hydropower and bioenergy, the development should be twofold the average of the last 5 years. But these implementation efforts are still far from the Net Zero Scenario trajectory.

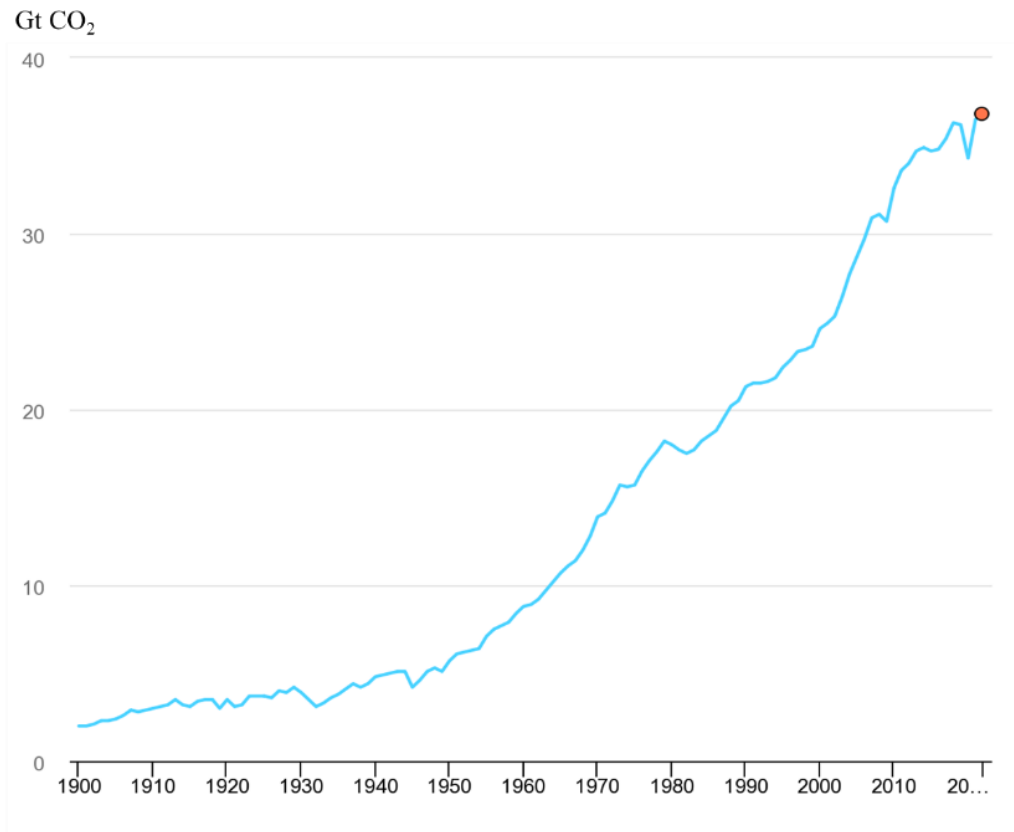


Figure I-2. Global CO₂ emissions from energy combustion and industrial processes, 1900-2022 [2].

Finally, there is a study [4] analyzing the main materials needed to generate low-emission electricity. Calculating the amount needed for the construction of new infrastructure and having Sustainable Development Goals Fund (SDG), goal 7, as a target for the transition to new, more sustainable and available energies can be an encouraging reason that the pathways can be viable in the medium and long term.

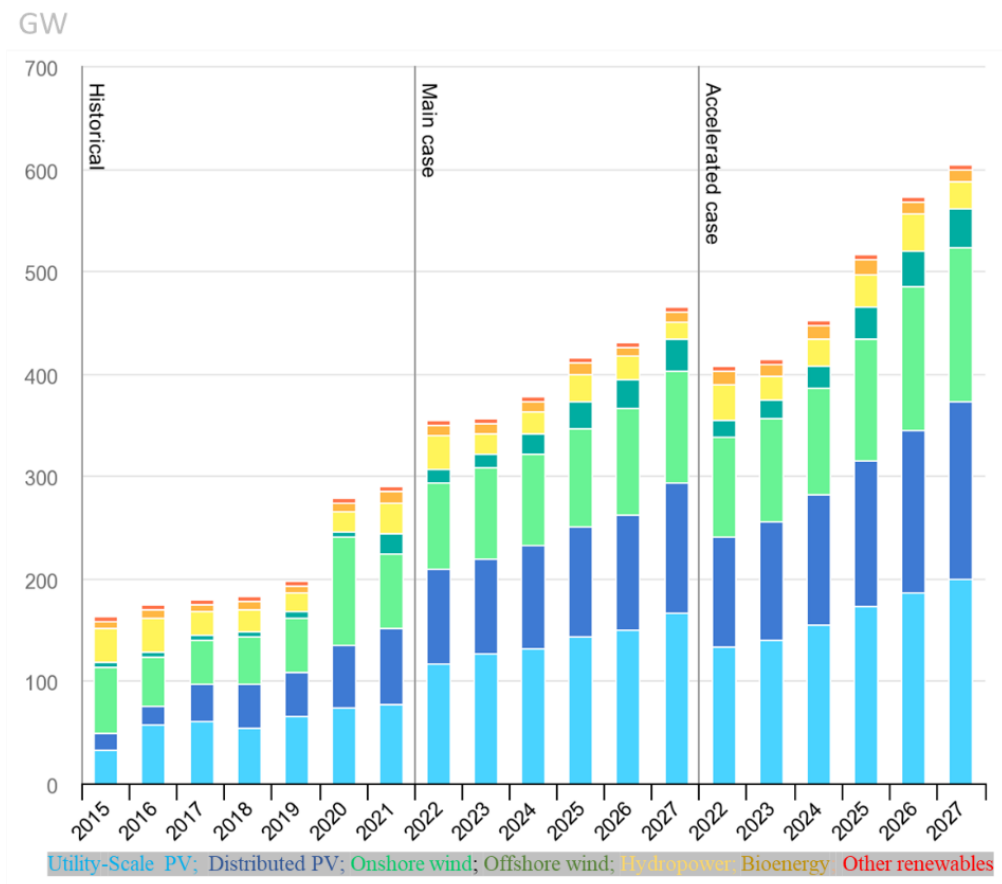


Figure I-3. Renewable annual net capacity additions by technology, main and accelerated cases, 2015-2027 [3]

I.2. Green methane: a renewable energy vector

Methane is, like hydrogen, extremely useful and investigated as a fuel and chemical feedstock. It is considered the second most important greenhouse gas contributor and relevant strategies to reduce methane emissions are a priority in the European Green Deal and the EU's methane strategy adopted by the European Commission [5]. The EU methane strategy's proposal for a regulation in the energy sector is a positive step towards reducing these emissions.

Oil and Gas Methane Partnership (OGMP) is a framework in the proposal on measurement and reporting of methane emissions towards improving the accuracy of

reporting and understating the source of emissions. The urgency reflected in the proposals on mitigation because methane has a much shorter lifetime in the atmosphere compared to carbon dioxide, but it is also much more portent as greenhouse gas.

It is also worth noting that the energy sector is not the only source of methane emissions, and efforts to reduce them should be extended to other sectors such as agriculture and waste management. However, the proposals in the energy sector are a positive step towards addressing methane emissions and can serve as a model for similar regulations in other sectors.

Depending on the origin of its production, methane can be considered under two different considerations: green methane or non-green methane.

Non-green methane coming from anthropogenic/natural sources (oil, natural gas, coal) is a source with near-term warming potential. Therefore, EU strategy aims to reduce this emissions being the EU as global leadership in this fight. Reducing emissions by 50% of anthropogenic consumption from 2020 to 2050, is expected to reduce the planet's global temperature by 0.2°C.

Green methane can be produced from anaerobic digestion of wastes producing biogas which is composed around 60% of methane or from other technological methods. Biogas is a mixture of CO₂, CH₄ and small quantities of other gases depending on the type of feedstock and the production pathway [7]. This digestion must be purified to obtain biomethane to finally, store it or introduce it into natural gas pipelines.

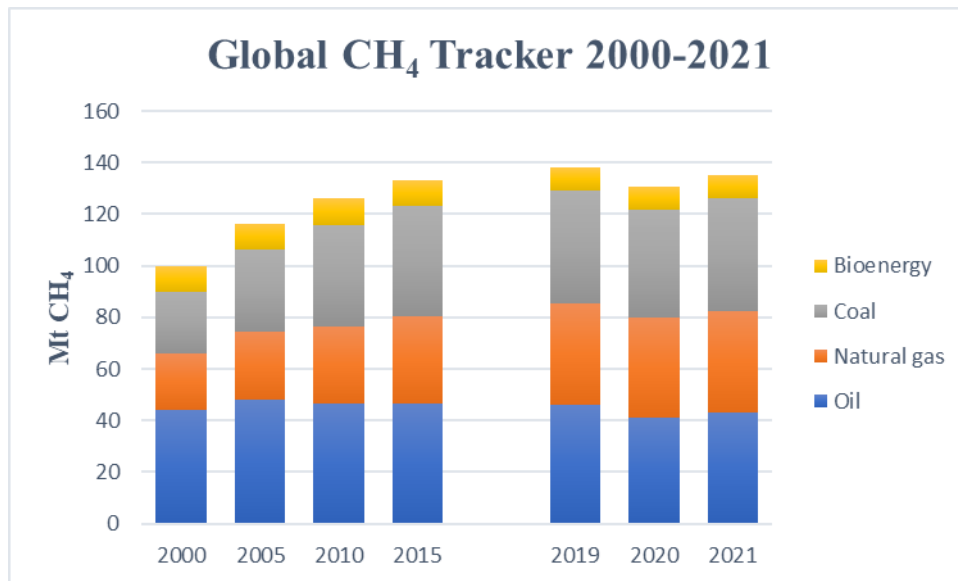


Figure I-4. Global methane emissions from the energy sector over time, 2000-2021 [6]

By 2050 EU's long-term decarbonization strategy is expected to grow between 54 and 72 Mtoe of biogas and biomethane the annual consumption, contributing towards the climate and EU's renewable targets [8].

Another pathway of obtaining methane in a renewable way and with high interest due to the use of CO₂ as a reagent, and thus mitigating the emission of this primary greenhouse gas emitted through human activities.

In fact, the production of renewable methane, unlike other high value-added raw materials such as hydrogen, would not require the implementation of new infrastructures for its transportation/storage and its use as a high value-added gas. Since it is a fuel with high production and use knowledge and lacks problems such as the embrittlement of materials, the research of new technologies for H₂ storage and transport such as liquid organic hydrogen carriers (LOHCs), and finally the development of technologies such as fuel cells for its energetic use.

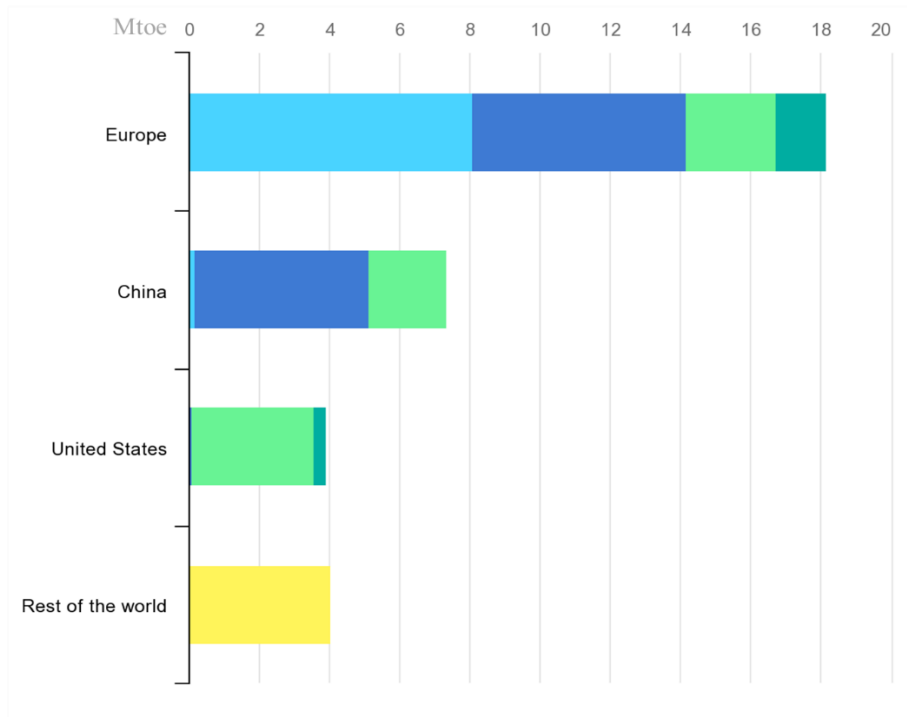


Figure I-5. Biogas production by region and by feedstock type [9]

I.3. Sustainable Development Goals (SDGs) Fund

Generally, all targets should undergo *The Sustainable Development Goals (SDGs)* which are a set of 17 global goals adopted by all United Nations member states.

Each goal has specific targets to be achieved by 2030, and progress towards achieving the goals is measured using a set of indicators. The SDGs are intended to be universal, meaning that they apply to all countries, regardless of their level of development. Succeeding the SDGs will oblige collective action and collaboration between states and individuals around the world.

A summary of the goals is listed below:



Figure I-6. 17 Image of the 17 Sustainable Development Goals.

- 1- **No poverty:** Globally, the number of people living in extreme poverty diminished from 36 % in 1990 to 10 % in 2015. The objective is ending poverty in all its forms everywhere by 2030.
- 2- **Zero Hunger:** Its goal is to end hunger, get food safely, improved nutrition, and endorse sustainable agricultural methods.
- 3- **Good health and well-being:** Its goal is to guarantee healthy living and promote wellness for everyone at all ages.
- 4- **Quality education:** Its objective is to safeguard inclusive and equitable quality education and support lifelong learning opportunities.
- 5- **Gender Equality:** Ending all forms of discernment against women, reject all practices of violence, eliminating all harmful practices, recognize and value unpaid care and domestic work and ensure women’s full and effective participation and equal opportunities are the main goals.

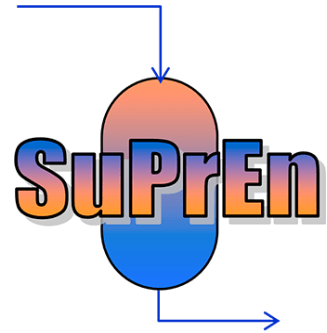
- 6- **Clean water and sanitation:** achieving universal, reasonable access and reasonably priced water for all, improving the quality of water and its management are some of the principal goals by 2030.
- 7- **Affordable and clean energy:** This objective has implications for the use of materials for research. In this field, materials with good-high availability are needed, as was the case with the shortage of batteries for electric vehicles. Geopolitical situations do not have a negative impact on both availability and final price. Therefore, international cooperation in the field of research must go hand in hand. This section is therefore essential if target goals want to improve the global energy efficiency rate, the expansion and improvement of infrastructures and current technologies. This goal is completely aligned with the PhD work as can contribute to generate affordable and clean energy like methane from renewables.
- 8- **Decent work and economic growth:** Promote sustained, inclusive and sustainable economic growth, full and productive employment and decent work for all.
- 9- **Industry, innovation and infrastructure:** The backbone of this objective is based on building resilient infrastructures, viable industrialization and fostering innovation.
- 10- **Reduced inequalities:** The reduction of inequalities and ensuring no one is left in terms of all policies and regulators involved.
- 11- **Sustainable cities and communities:** The goal states that, by 2030, cities and human settlements should be inclusive, safe, resilient and sustainable. By 2050, 7/10 of the world's population is expected to live in urban areas.

- 12- **Responsible consumption and production:** It aims to guarantee sustainable consumption and production outlines globally. It calls for all countries to take steps to carry out a 10-year framework of programmes on sustainable consumption and production, with developed countries taking the lead and into account the development and capabilities of advanced countries.
- 13- **Climate action:** This goal aims to strengthen resilience and adaptive capacity to climate-related hazards and natural disasters worldwide, integrate climate change measures into national policies, strategies, and planning, and enhance education, awareness and human and institutional capacity for climate change mitigation, adaptation, mitigation and early warning.
- 14- **Life below water:** This international agreement describes the right and responsibilities of each government in their use of the oceans, launching plans for trading, the environment and the managing of natural resources.
- 15- **Life on land:** There are a set of goals set by the UN to ensure the conservation and sustainable use of the Earth's ecosystems, biodiversity, and natural resources, and to promote sustainable development.
- 16- **Peace, justice and strong institutions:** It is focused on promoting peaceful and inclusive societies, providing access to justice and building real and accountable institutions.

References

- [1] Commission, E. (n.d.). Bruselas, 28.11.2018 COM(2018) 773 final.
- [2] IEA, Global CO₂ emissions from energy combustion and industrial processes, 1900-2022, IEA, Paris <https://www.iea.org/data-and-statistics/charts/global-co2-emissions-from-energy-combustion-and-industrial-processes-1900-2022>, IEA. Licence: CC BY 4.0.
- [3] IEA, Renewable annual net capacity additions by technology, main and accelerated cases, 2015-2027, IEA, Paris. <https://www.iea.org/data-and-statistics/charts/renewable-annual-net-capacity-additions-by-technology-main-and-accelerated-cases-2015-2027>, IEA. Licence: CC BY 4.0.
- [4] Wang, Seaver, Hausfather, Zeke, Davis, Steven, Lloyd, Juzel, Olsen, Erik, Liebermann, Lauren, McBride, Jameson, & Núñez-Mujica, Guido. (2022). Materials demand for electricity in climate mitigation scenarios. <https://doi.org/10.5281/zenodo.7023703>.
- [5] Brussels, 14.10.2020 COM(2020) 663 final.
- [6] IEA, Global methane emissions from the energy sector over time, 2000-2021, IEA, Paris <https://www.iea.org/data-and-statistics/charts/global-methane-emissions-from-the-energy-sector-over-time-2000-2021>, IEA. Licence: CC BY 4.0.
- [7] IEA (2020), Outlook for biogas and biomethane: Prospects for organic growth, IEA, Paris <https://www.iea.org/reports/outlook-for-biogas-and-biomethane-prospects-for-organic-growth>, License: CC BY 4.0.
- [8] Brussels, 28.11.2018 COM(2018) 773 final <https://eur-lex.europa.eu/legal-content/EN/TXT/?uri=CELEX:52018DC0773>.

[9] 2018 IEA, Biogas production by region and by feedstock type, 2018, IEA, Paris
<https://www.iea.org/data-and-statistics/charts/biogas-production-by-region-and-by-feedstock-type-2018>, IEA. Licence: CC BY



Rafael Canales Larrazabal
Bilbao, 2023



Universidad
del País Vasco

Euskal Herriko
Unibertsitatea

MDe

Master eta Doktorego Eskola
Escuela de Máster y Doctorado
Master and Doctoral School

CHAPTER II

STATE OF ART

CHAPTER II. STATE OF ART

As previously specified, Chapter II contextualizes the methane production via several technologies. The point of interest is the production of renewable energy sources for the production of fuels like methane of high interest due to its storage capacity and transport and energy density. At this point, previous results related to other publications are shown regarding Sabatier Reaction in thermochemical and photocatalytic processes.

II.1. CH₄ production directly from biogas

Methane can indeed be produced directly from biogas through a process called anaerobic digestion. Biogas is generated from the breakdown of organic matter in the absence of oxygen, which commonly occurs in environments like landfills or wastewater treatment plants.

During anaerobic digestion, the biogas produced is collected and undergoes a treatment process to eliminate impurities, such as carbon dioxide and hydrogen sulfide. The purification process helps to achieve a high purity methane, resulting in a high-quality methane gas stream.

The resulting biomethane can then be utilized as a renewable energy source. It can be employed for electricity generation by burning it in a gas turbine on the Brayton cycle as an example of energy generation. Additionally, it can serve as a vehicle fuel, either in compressed natural gas (CNG) form or as a component - renewable natural gas (RNG).

One significant benefit of this process is its positive environmental impact. By confining and using CH₄ that would be emitted into the atmosphere, the anaerobic digestion of

biogas helps to mitigate greenhouse effects. Hence, the conversion of biogas into methane through anaerobic digestion not only yields a renewable energy source but also contributes to a reduction in greenhouse gas emissions, especially when it results in the production of other valuable by-products.

II.2. Power-to-Gas (PtG)

The Power-to-Gas (PtG) concept is a promising technology which uses surplus or renewable electricity to produce H_2 via water electrolysis which is currently predominating or via thermal decomposition (thermochemical cycles), which can be finally converted into various energy carriers, such as renewable methane which is the goal of this thesis, or synthesis gas, electricity, other hydrocarbons, etc. PtG provides a long-term storage solution for excess electricity, reduces the load on the smart electric grid, and produces renewable fuels for transportation/storage (e.g. LOHC technology), household natural gas consumption, industry and chemical potential energy store as depicted in Figure II- 1.

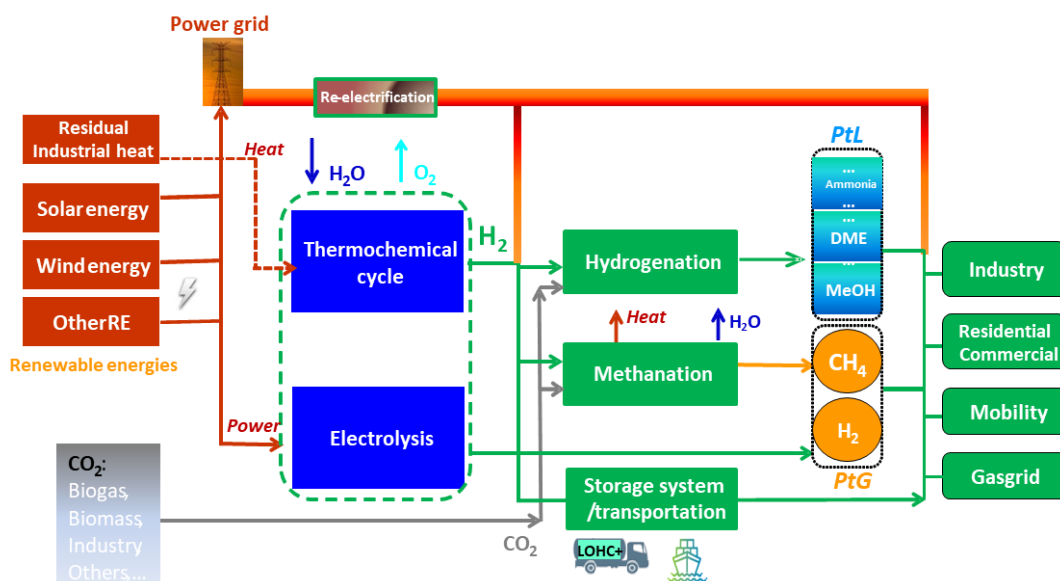


Figure II- 1. Power-to-Fuel scheme

In Regensburg (Germany) technicians from OTH reviewed the world's existing PtG projects with 56 H₂ and 38 CH₄ projects active in 2019 [1,2].

One of these projects is the "WindGas" project in Hamburg-Reitbrook (Germany), which was inaugurated on Oct. 15, 2015 and produced renewable hydrogen through electrolysis using excess wind power. The hydrogen was then injected into the natural gas grid, providing a renewable energy source for heating and transportation.

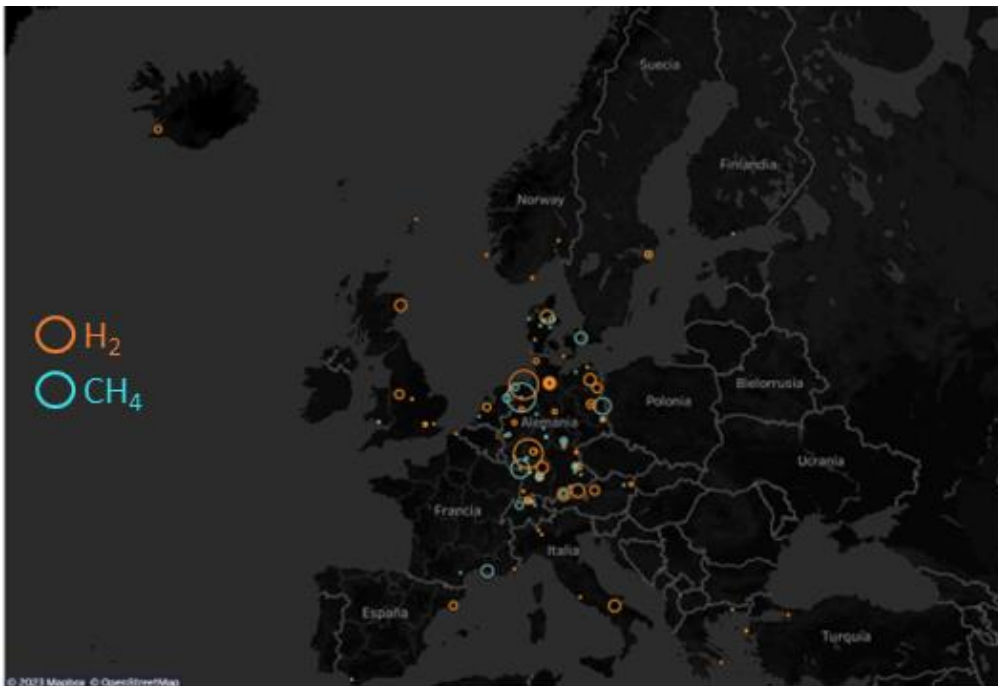


Figure II- 2. Existing Power-to-Gas Projects Worldwide as of September 2019. Source: Technical University of Applied Sciences (OTH)/POWER magazine.

Another project coordinated by ENGIE and supported by France Governments is called, "GRHYD", which was launched in 2014 and aimed to develop a complete PtG system, including hydrogen production through PEM electrolyzer, injection of hydrogen into the territory's natural gas pipelines, and use of hydrogen in terms of domestic use. This

project successfully produced and injected renewable H₂ into the already existed gas pipelines, demonstrating the potential for scaling-up renewable gas production.

In the case of the Netherlands, "Gasunie" is working on various forms of energy: Green Gas, Hydrogen, Heat and Capture & Reuse of CO₂. Currently, the main gas used for large-scale transport and storage is natural gas, but they are focus also on green gases and hydrogen.

Other notable PtG project in Europe includes the "SmartHyFlex" project in Denmark, which aims to produce renewable hydrogen and synthetic methane through electrolysis and methanation, and the "Haeolus" project in Norway, which aims to produce hydrogen from wind power and store it underground in salt caverns in order to use in fuel cells.

Overall, these PtG projects demonstrate the potential for renewable gas production and injection into existing gas infrastructure, providing a flexible and sustainable solution for energy storage, transport and heating. As renewable energy sources continue to grow, PtG technology is anticipated to have a significant role in enabling a more sustainable energy system in Europe and beyond.

II.2.1. Hydrogen production via water electrolysis

Hydrogen demand in 2021 reached 94 Mt principally from traditional uses in refining, industry and new applications such as new steel projects for iron reduction, new means of air, maritime and land transport sectors. As most hydrogen technologies depend on electricity mainly from renewable sources, the price for production-storage and distribution will depend mostly on the electricity pool price. The cost of hydrogen

manufacturing could oscillate from 3-4 €/kg till 10 €/kg. Therefore, technological advances in the efficient production of hydrogen will have a more competitive price in the future and improve the supply-demand of other energy carriers [3].

Considering guidelines and actions that governments around the world the estimation analyzed by IEA is that H₂ claim could reach 115 Mt by 2030. This equivalences with the 130 Mt that would be desirable to reach existing climate pledges stated by governments worldwide, and with approximately 200 Mt required by 2030 to be on course for net zero emissions by 2050.

At present, the most current process for obtaining hydrogen is referred to as, Water electrolysis which consists on an endothermic process of splitting H₂O into H₂ and O₂ through a flow of electric charge. The process consists of passing an electric charge through water, which separates H₂O into hydrogen ions (H⁺) and negatively charged ions (OH⁻). H⁺ are moved to the cathode and gain electrons, which converts them into H₂. At the same time, OH⁻ are attracted to the anode and lose electrons, which converts them into oxygen gas (O₂).



Figure II- 3. Battery electric and fuel-cell electric vehicle (BMW X5 prototype)

The overall reaction can be represented as:



However, water electrolysis is an energy-intensive process, and the cost of producing hydrogen by this method can be relatively high. Therefore, researchers are exploring new methods and materials to make the process more efficient and cost-effective.

Three different H_2 production technologies are mentioned below. Alkaline based electrolysis (AECs) which is the most common technology, but proton exchange membrane (PEMECs) electrolysis and solid oxide electrolysis cells (SOECs) are developing technologies [4–8].

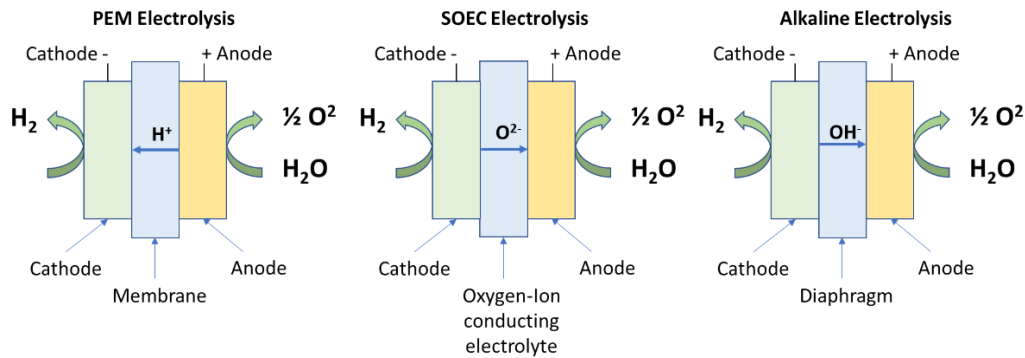


Figure II- 4. Type of water electrolyzers

SOECs are considered as the greater electrical efficiency, but are the least developed having challenges with corrosion, seals, thermal cycling and chrome migration [9].

Some of operation properties are listed below:

- **High Operating Temperature:** The SOEC operates at a higher temperature range of 700 to 900 °C. This high temperature promotes fast reaction rates compared to PEMECs and AECs. Faster reaction rates result in higher efficiency and faster production of hydrogen gas.
- **Lower Operating Voltage:** Due to the high operating temperature, they can achieve a lower operating voltage of 1.2 to 1.4 V.
- **Reduced Energy Consumption:** The lower operating voltage translates into less energy consumption during hydrogen production. Since electricity costs constitute a significant portion of the overall H₂ production cost, the SOEC's thermodynamic advantages contribute to lower unit hydrogen production costs.
- **Economic Advantage:** The combination of fast reaction rates, lower operating voltage, and reduced energy consumption directly leads to an economic advantage for the SOEC.

PEMECs are more efficient than AECs, without corrosion and seals issues that SOECs and can stand for load of transients revealing faster start up performance but more costly than AECs. The drawbacks are the short duration of the membrane, the small capacities available and the high costs associated with the use of noble metal catalysts. For the time being (2019), PEMECs are in a temporary commercial state and have a lower efficiency and short duration than AECs, but from a global perspective, the efficiency is expected to surpass that of AECs [10].

Finally, AECs are the most investigated and the cheapest but with the lowest efficiency and thus, the highest electricity costs [11].

II.2.2. CO₂ removal from air

Carbon dioxide removal technologies, also known as carbon removal or negative emissions technologies, are methods and processes designed to capture and remove CO₂ from the atmosphere. These technologies are critical in the fight against climate change, as they can help to reduce the concentration of CO₂ in the atmosphere, which is a major driver of global warming. The primary advantage of CO₂ capture is its potential to reduce greenhouse gas emissions, particularly CO₂ that could be integrated with existing industrial infrastructure. However, operational costs still are too high and further developments are needed. In the case of the membrane technology, it has shown promise in addressing challenging separations, including the removal of carbon dioxide, sulfur dioxide, and nitrogen oxides from flue and waste gases. These membranes selectively allow CO₂ to permeate through while blocking other gases like nitrogen or oxygen. The captured CO₂ can then be recovered for storage or utilization purposes.

Firstly, the advantages of different membrane-based for CO₂ with high permeability based on different materials are going to be detailed. Polymer membranes are relatively inexpensive to produce and can be easily scaled-up, with possibility of operating at low temperatures which can lead to energy savings and their microporous structure leading to a high permeability, enhancing solubility and selectivity to CO₂ (14.3 of CO₂/N₂ Selectivity). Mixed-matrix membranes (MMMs) improve some properties of the polymer membranes adding filler materials into polymer membrane improving affinity, the diffusivity and mechanical stability and CO₂/N₂ selectivity by 68 %; and finally, the facilitated transport membranes which enhance 90% CO₂/N₂ selectivity and more than 50% CO₂ permeability due to its high CO₂ permeability and potential for energy efficiency operating at lower temperatures and pressure differential compared to traditional methods [12].

The main drawbacks for polymeric membranes are the limited chemical resistance, temperature and pressure constraints, plasticization and membrane aging. The disadvantages of mixed-matrix membranes are the particle sedimentation, inter-facial voids and filler-polymer incompatibility. And finally, the facilitated transport membranes have low stability, carrier leakage and saturation of the carrier.

Lakshminarayana Bhatta et al. studied promising materials using hydrotalcite materials combining with metal-oxides for CO₂ capture. [13]. Hydrotalcites are superior to other materials due to high selectivity for CO₂ chemisorption and good regenerability. The number of strength basic sites for improving CO₂ sorption can be modified by controlling the number of defects of the material like adding zeolites. The sorption capacity (wt% of CO₂) combining hydrotalcites coated with zeolites was 30.8% using

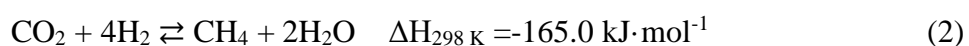
100% of pure CO₂ if they are compared with other promoters such as K-Na (5.3 %) or non-modified hydrotalcites (7.0 %). The major disadvantage is the adverse effect of water vapor in sorption stability and high cost of the material due to zeolites addition.

Additionally, M.R. Rahimpour et al. studied the different effects for CO removal connected with hydrogen permselective membrane reactor to methanol production with high CO conversion and H₂ permeation rate [14]. Further research such as the combination of CO₂ at low pressure and its subsequent hydrogenation process for the production of methanol [15].

II.2.3. CO₂ Methanation

CO₂ methanation according to Sabatier Reaction, is a chemical reaction that converts carbon dioxide and hydrogen into methane and water in the presence of a catalyst. This reaction can be used as a form to store renewable energy into CH₄, which can be used as a fuel or feedstock for the production of chemicals. Carbon dioxide could be extracted from the atmosphere so the balance of carbon emission would be zero [16].

The reaction can be represented by the following reaction (Equation 2):



The reaction is highly exothermic, and thermodynamically favorable at low temperatures. The process is typically carried out at medium range temperatures (250-400°C) and high pressures (1-50 bar) with active catalysts to increase the reaction rate and yield.

In Sabatier reaction, several cooling stages are normally required after each reactor to condense the H₂O produced during the reaction and increase the methane yield. This is because the formation of water is an equilibrium-limited step in the reaction and

removal of water from the reaction mixture shifts the equilibrium toward the formation of more CH₄.

There are two main reaction pathways proposed for the Sabatier process [17,18]. The first, is the dissociation of CO₂ to CO (Equation 3) and later hydrogenation of CO to CH₄ (Equation 4). Apart from those mentioned, there is also a secondary reaction that also occurs, the water-gas shift (WGS) reaction (Equation 5):



The thermal energy generated during the methanation process and cooling stages can be integrated into external processes, such as power generation or heat utilization, to advance the overall energy efficiency of the system. Recirculating part of the cooled gas stream back to the reactor can also help improve conversion rate by increasing reactant concentration and reducing cooling requirements.

Currently, the implementation of different stages involving CO₂ capture and methane production has been investigated. CO₂ capture is typically performed using technologies like absorption, adsorption, or membrane separation [12,19]. An interesting combination of CO₂ capture and the reduction is becoming urgent and recent projects using electrocatalyst for electrochemical CO₂ reduction reaction with the advantage and drawbacks involved for scaling up are challenges for the short term [20].

II.3. Power-to-Liquids (PtL)

Currently, there are processes in which the products generated are liquid as a competitor of Power-to-Gas generated from renewable sources. This process typically involves several steps and can produce synthetic fuels such as hydrogen, ammonia, or synthetic hydrocarbons like gasoline, diesel, or kerosene. Power-to-liquids is seen as a way to address some of the challenges associated with energy storage and transportation in a sustainable manner. Under the same reagents for methanation, methanol, also called Power-to-methanol, can be obtained as an alternative route.

Power-to-methanol (PtM) is a process that involves converting electrical energy into methanol, a chemical compound used as a fuel or feedstock in various industries. The PtM process typically consists of two main steps: electrolysis (same as Power-to-Methane) and methanol synthesis or CO₂ hydrogenation to methanol. Syngas is a mixture of CO, H₂, and CO₂, along with small amounts of CH₄, H₂O, and other impurities.

The production of methanol from syngas involves a series of equilibrium reactions. The typical reactions involved are the following: Water-Gas Shift Reaction (Equation 6) and Methanol synthesis (Equation 7).



At this point some heterogeneous and homogeneous catalysts at low temperature have been investigated below 30 °C [21,22]. On the other hand, the general equation for the hydrogenation of CO₂ to CH₃OH is as follows (Equation 8):



Currently, some researchers emphasized the use of Cu and Pd-based catalysts from 200 to 300 °C and high pressure (30-100 bar) [23].

Nevertheless, different pathways have been investigated for alcohol, ether and hydrocarbon with the usage of both H₂ and CO₂. A good summary selected by Steffen et al. [24] scheme involving all reactions is depicted below:

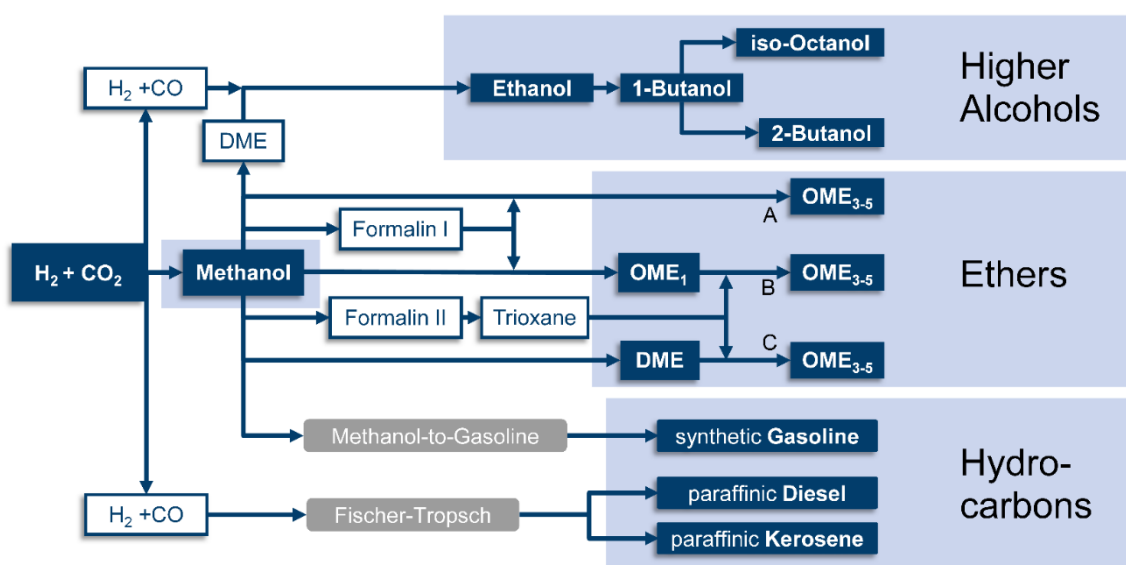


Figure II- 5. Selected synthesis pathways for H₂+CO₂ [24]

II.4. Reactors for Sabatier process

II.4.1. Fixed bed reactor

In a fixed bed reactor, the solid catalyst is generally held motionless in a bed while the reactants are passed through the bed at a distributed reaction manner for the reaction. The catalyst bed may consist of one or more layers of catalyst particles previously analyzing the appropriate particle size, which may be mixed by a temperature homogenizing material such as silicon carbide. One of the perks of fixed-bed reactors is

that they can operate at high operational conditions, which can enhance the reaction rate and the selectivity. Andre Bolt et al. designed a new helical fixed bed type reactor [25] or the effect of alternatively feeding reactants [26]. Depending on the external or internal cooling conditions in the reactor itself are referred to as adiabatic or isothermal respectively.

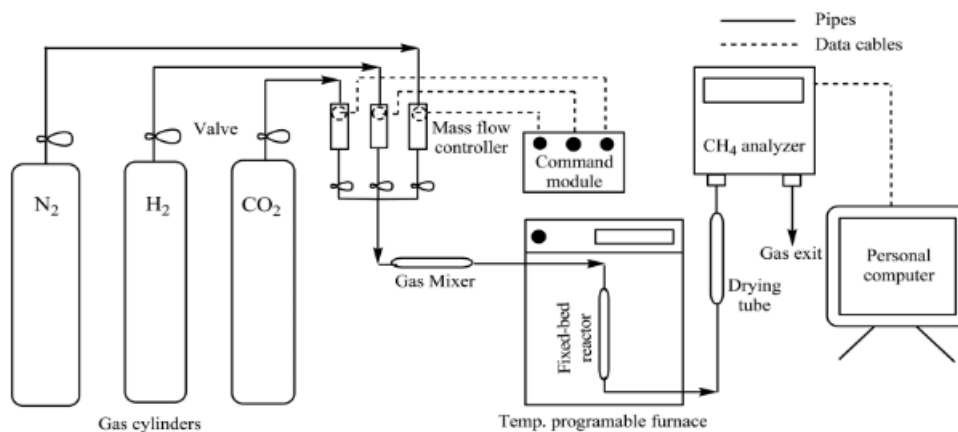


Figure II- 6. Scheme of a fixed bed reactor for CO₂ methanation [27]

The first one is normally arranged in series (2-5 reactors), the temperature profile is different due to the different concentrations of reactants affected by Le Chatelier. Therefore, successive cooling to improve thermodynamically the Sabatier reaction and, as a consequence of the cooling, to obtain a higher quantity of water by condensation, improves the final methane production. On the other hand, isothermal reactors, when subjected to internal cooling, are more favorable to methanation. As an improvement to this type of reactor, the solid-gas contact can be enhanced by improving heat transfer and reducing the pressure drop with respect to the introduction of powder catalyst by impregnating a catalyst on monoliths or foams (ceramic or metallic materials) as shown in Figure II- 7 B. The novel of using smaller reactors improving at same time the energy consumption and efficiency is called as process intensification.

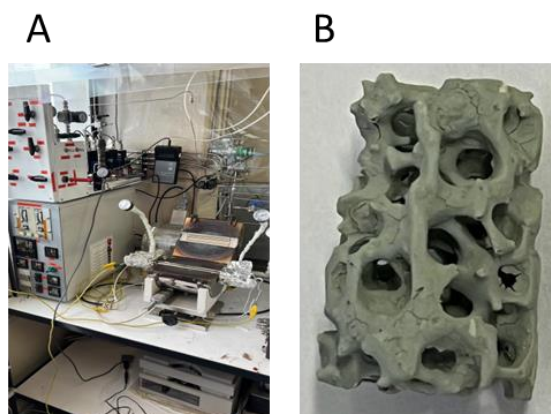


Figure II- 7. A) Fixed bed reactor used in the CNR-ITAE. B) Commercial catalyst impregnated on alumina open cell foam

II.4.2. Fluidized bed reactor

These type of reactors solve the problems of the fixed-bed-reactors due to a better distribution of the catalyst inside the reactor and therefore provide a greater surface interaction with the fluid (gas or liquid). Fluidized bed reactors are a promising technology for methanation applications due to their ability to provide homogeneous temperature conditions, efficient heat transfer, and flexibility in handling varying flowrates. The use of internal heat exchangers allows for precise temperature control and avoids common issues associated with exothermic reactions. However, their design requires careful consideration of heat management and bed fluidization to optimize performance in methanation processes.

Maxime Hervy et al. demonstrated the efficiency of this type of scale up reactor associated with a PtG production [28].

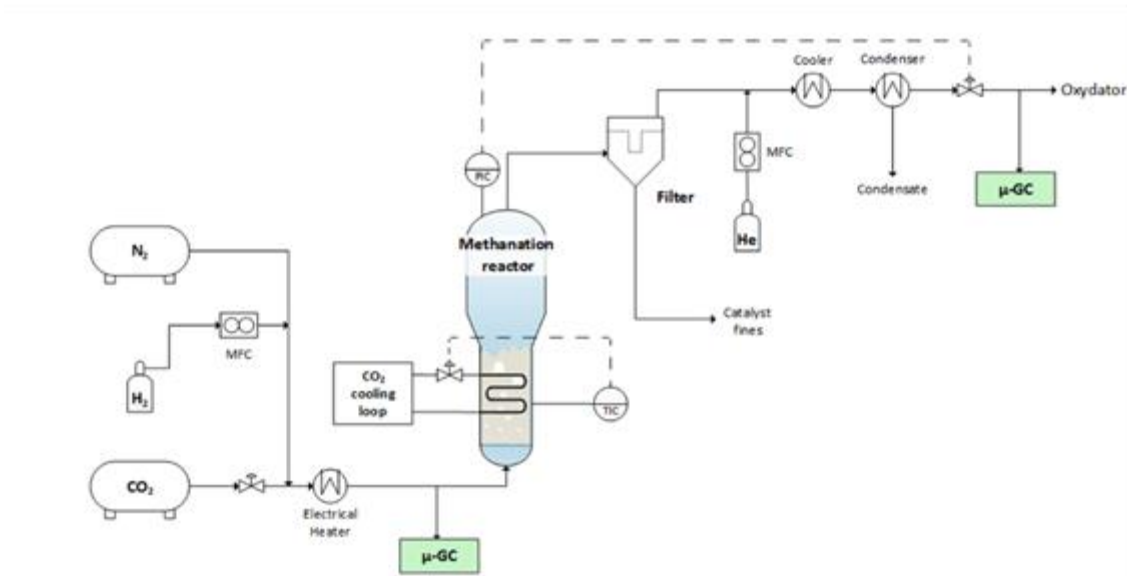


Figure II- 8. Fluidized bed reactor for CO₂ methanation on the Gaya platform [28]

II.4.3. Three phase reactor

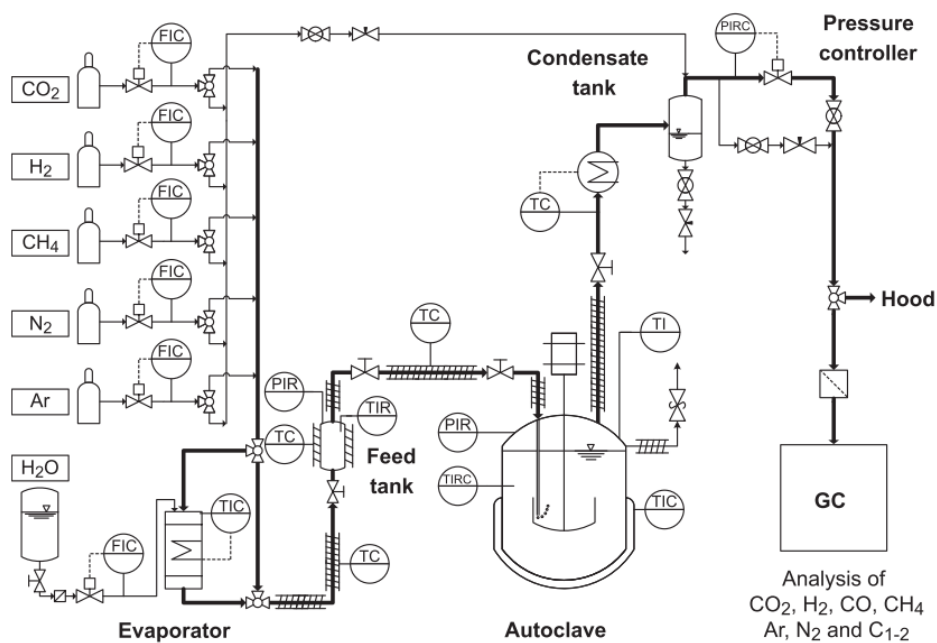


Figure II- 9. Scheme of a three-phase reactor for CO₂ methanation [29]

A three-phase reactor for CO₂ methanation is a type of chemical reactor designed to accommodate three distinct phases: gas, liquid, and solid. The gas phase consists of the

gaseous reactants, CO₂ and H₂. These gases are introduced into the reactor, and the reaction takes place in the presence of a solid catalyst dispersed by the fluid. The liquid phase primarily contains H₂O as a byproduct of the reaction but, depending on the specific reactor design and conditions, other liquid components (e.g., dibenzyltoluene) may be present.

The presence of a liquid phase can influence the reaction kinetics and heat transfer. Determining the kinetics of CO₂ methanation in a three-phase system, as mentioned earlier, can be challenging due to the complex interplay of gas and liquid phases. Lefebvre et al. studied the reaction kinetics which are influenced by different gas solubilities and the different liquids applied to the reactor [29].

II.4.4. Photocatalytic reactor

Photocatalysis has gained a lot of attention converting solar energy to value-added products in the presence of a light source and a photocatalyst. At same time two different reaction pathways can take place: thermocatalytic and photocatalytic reaction (non-thermal). Many different reactor designs have been investigated depending on the reaction process but small number have been scaled up due to three aspects: (1) problems associated with irradiance; (2) reproducibility of catalyst loading and distribution into the reactor and (3) less surface area of incident light is available when the photocatalyst is supported on a material such as foams or monoliths (poor light distribution). In this thesis a new reaction process has been investigated with a commercial photocatalytic reactor as shown in the Figure II- 10 with heterogeneous photocatalysts.



Figure II- 10. Harrick commercial photoreactor

The key goal of photocatalytic reactions is to achieve continual improvements in the catalysts' sensitivity to sunlight. As seen in Figure II- 11, most solar radiation energy is in the visible region, so one desirable innovation is the use of photosensitive catalysts in this region. In our study, we developed catalytic systems that present a different band gap, which was confirmed by their light absorbance and reflectance (Tauc plots). In terms of light source, the influence of different energetic wavelengths can be analyzed. The photon flux provided by the light irradiance, accelerates reaction rate when the photon energy is adequate for the photo-behavior of the catalyst.

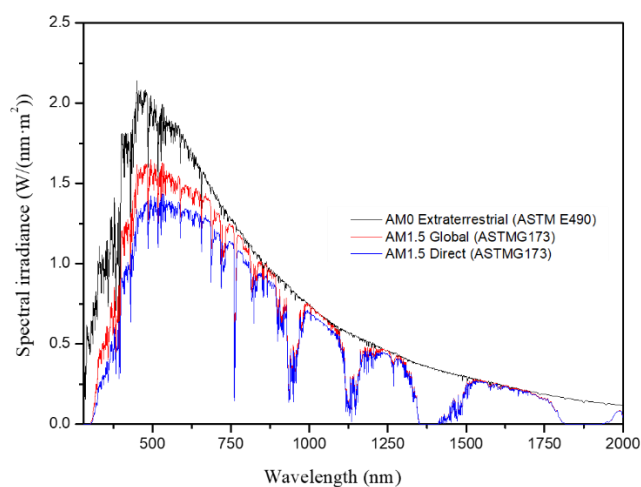


Figure II- 11. Standard solar spectra for space and terrestrial use

However, this reaction takes place only on the illuminated part, while on the unexposed side, the conventional (non-light) reaction predominates. Mainly, semiconductor materials are used as photocatalysts at present. Pairs of electron-hole are excited when the charge carriers generated in the semiconductor have sufficient energy provided by the light source. When it is irradiated, the electrons move from the valance band suffering a charge separation resulting in the formation of an electron-hole recombination [30].

A fast recombination of energy transfer negatively affects the activity due to the dissipation of the energy adsorbed or migrate to the surface starting an oxidation-reduction process with the chemical reaction (CO₂ reduction). To avoid deactivation of the catalyst, a sacrificial electron donor must take place (H₂). This excited electrons can jump up from the conduction band of the semiconductor into the noble/non-noble metal nanostructures for an efficient separation of the photogenerated electrons and holes which are trapped by the metal nanostructures and thus, limit the recombination process.

Depending on the metallic nanostructure investigated, the shape, size, composition and dielectric environments, affect the electron oscillation due to the electric field generated by the light absorption. This physical phenomena is called as localized surface plasmon resonance (LSPR) and excites conduction electrons of the metal, enhancing electric fields in the external surface of the nanostructures contributing to chemical photo-driven reactions [31]. Two mechanisms take place depending on the LSPR adsorbed energy: non-radiative decay (hot electrons-holes) and near-field enhancement as shown in Figure II- 12.

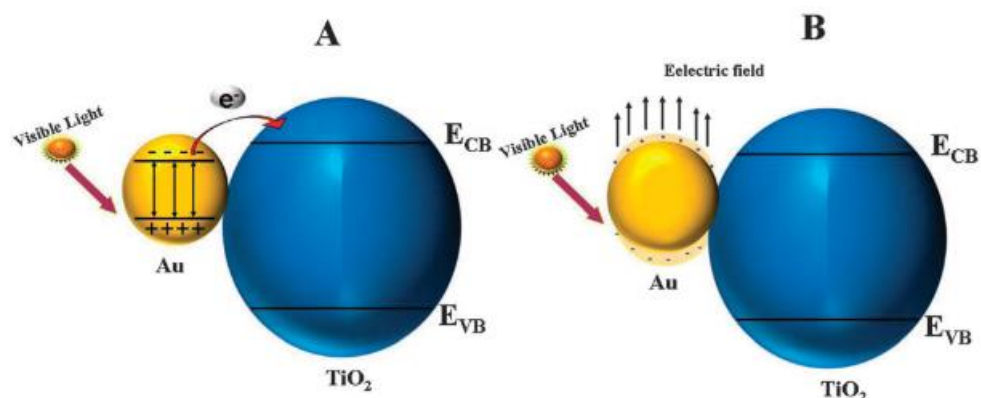


Figure II- 12. A) Charge transfer mechanism; B) local electric field enhancement mechanism [32]

II.5. Critical raw materials

Global investigation is aware of the use of critical raw materials which are essential for the development of key technologies, playing a crucial role in achieving the SDGs. The supply of critical raw materials is sometimes concentrated in a small number of countries, which can create dependence on those countries and increase the risk of supply disruptions. For this reason, there is increasing interest in developing alternative sources of these materials. In 2023, the EU updated the list of raw materials considered.

In this thesis, materials considered as critical according to the list of critical raw materials in Annex II, section 1 of the Regulation proposal COM(2023) [33] are listed below:

Table II- 1. CRMs used during the PhD thesis

1-Cerium (Light Rare earth metal)	2-Cobalt	3-Magnesium	4-Gold
5-Nickel	6-Titanium metal	7-Molybdenum	

Efforts are also being made to improve catalyst recycling and recovery to reduce the dependence on new raw materials and minimize the environmental impact of catalyst production and disposal. Additionally, research into new catalyst materials and innovative reactor designs may help mitigate the potential supply chain risks associated with critical raw materials in CO₂ methanation and other catalytic processes.

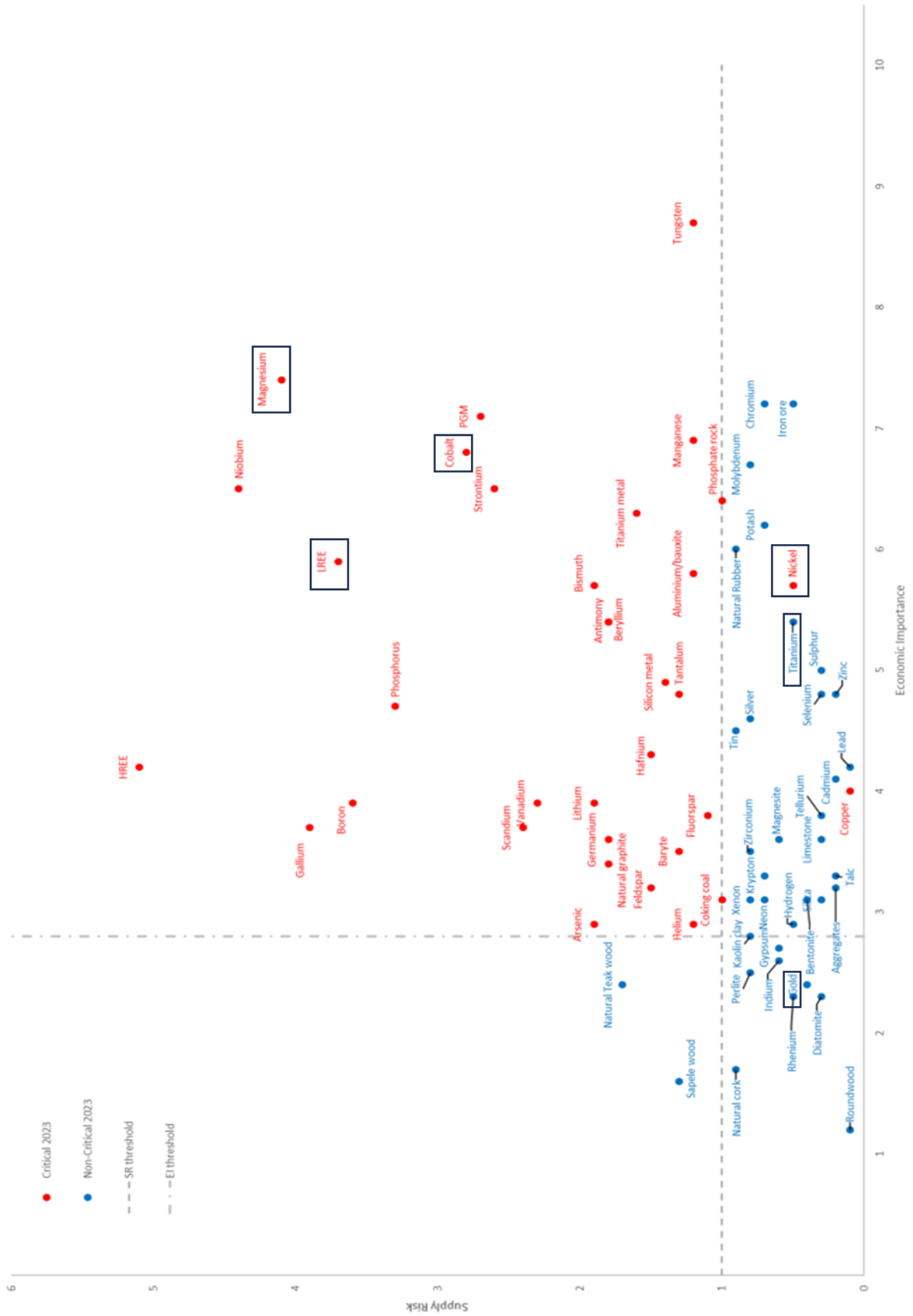


Figure II- 13. Results of the 2023 EU criticality assessment [34]

II.6. Sabatier reaction catalysts

II.6.1. Noble and non-noble metal catalyst

Noble and non-noble metal catalysts are two broad categories of catalysts used in various chemical reactions. Regarding noble metals, Leonardo Falbo et al. Studied the reactivity of Ru supported on alumina catalyst in the hydrogenation of CO/CO₂ gas stream. Catalyst was highly selective in the CO₂ methanation and stable but with the existence of CO at low temperatures prompt to a lower CO₂ conversion and a progressive deactivation [35]. Other authors synthesized bimetallic Ru-Ni/ Ru-Ce catalysts with promising results [36,37].

Non-noble metals are used due to the cheaper cost and abundance. Nickel shows high activity but it tends deactivates easily [38–40]. Cobalt has higher resistance towards sintering [41,42]. Iron presents high activity but low selectivity to methane [43].

Nobel metal such as silver was used for CO₂ conversion to enhance activity due to its photo-response as it improves bimetallic Ni-Ag interaction under laser irradiation [44]. Gold interaction on different metal oxides induced methanation reaction at lower temperatures compared with convectional Sabatier reaction [45,46]. Platinum is selective to CH₄ formation due to the previous formation of CO adsorbed species on this metal [47].

The activity comparing different metals for CO₂ methanation was analyzed by Younas et al as follows [27]:

Activity	Ru>Rh>Ni>Fe>Co>Os>Pt>Ir>Mo>Pd>Ag>Au
Selectivity	Pd>Pt>Ir>Ni>Rh>Co>Fe>Ru>Mo>Ag>Au

II.6.2. Supports

The most investigated supports for methanation process are: Al₂O₃ mostly used in γ -phase [35,40,41,48], SiO₂ [49–51], ZrO₂ [52,53] and CeO₂ [54–57] which were synthesized with the addition of nickel as active phase.

Zeolites were also reported as a promising structure for the research of active metal-based zeolites [58,59] for Sabatier process. But characteristics such as low cost, the insolubility of the material in water and its high anticorrosive stability during photocatalytic reactions make this material suitable for use in methanation. It also depends on the treatment to which the material is subjected, the 4 different polymorphs are important in terms of photocatalytic behavior, such as anatase, rutile (most stable in bulk), brookite and the monoclinic TiO₂. Noble metals and a mixture of TiO₂ with metal oxides acting as co-catalyst are often used for reducing electron-hole recombination effect [30,60].

II.6.3. Hydrotalcites

Currently, hydrotalcites-derived materials (HTCs) have several uses in the field of fuels, such as CO₂ capture and storage, the conversion of natural gas, the mitigation of pollution, etc. As natural minerals (Figure II- 14), hydrotalcites belong to a class of anionic and basic clays with a general structure of $[(M^{2+})_{1-x} (M^{3+})_x] (An^-)_{x/n} zH_2O$, in which M represents the divalent or trivalent metal cations, An⁻(CO₃⁻, Cl⁻, NO₃⁻) represents the anions of the interlayer, and $x (M^{3+}/M^{3+} + M^{2+})$ is the molar ratio, which is normally fixed between 0.25 and 0.33.

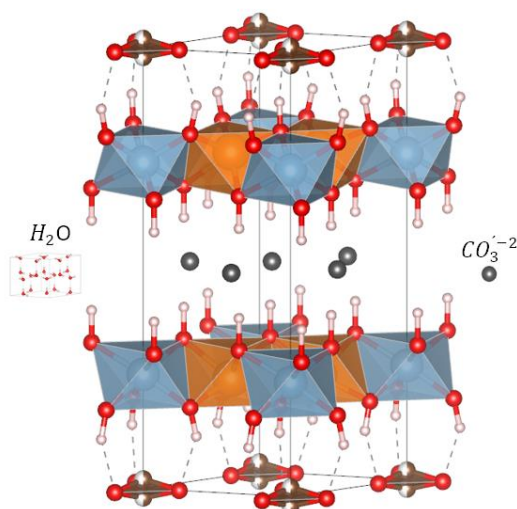


Figure II- 14. Scheme of the structure of the hydrotalcite

The partial substitution of divalent or trivalent cations with a different nature in HTC's can modify the structure, generating interesting properties, such as the modification of the specific surface area, the addition of structural defects, the enhanced dispersion of active metals, and improvements in acidic–basic structural sites, which might enhance the hydrogenation of CO_2 [61–64].

II.7. Structured catalysts supported on foams

Structured catalysts are designed with active catalytic components supported on specific geometric structures, such as ceramic honeycombs or foams [65]. These structured supports offer several advantages over conventional fixed bed reactor as process intensification with an efficient heat and mass transfer properties with higher catalytic performance. Firstly, an appropriate catalysts must be selected. Optimizing the catalyst composition and structure is essential for intensifying the wash-coating process. The rheological behavior for dip-coating process affecting the slurry's viscosity is correlated to the thickness of the catalysts loaded on the foam surface and to the mechanical stability of the structured materials.

II.8. Summary of current the catalytic and photocatalytic catalysts

A summary of the methanation results under conventional catalytic (non-light) and photocatalytic conditions is shown below. Table II- 1 provides a short summary of the materials investigated and the reaction conditions applied. As can be observed, the most common supports are alumina, titania, and ceria, and the main metals are gold, ruthenium, and nickel, among others, normally at temperatures between 523 and 573 K. The use of noble metals must be avoided because of their price and availability. Regarding precedents in terms of the reaction mechanism, the role of the plasmon resonance band, the average particle size, and the replacement of metal oxides acting as support changing, the valence-conduction band energy and the CO₂ adsorption capacity are the main characteristics that enhance the activity of the dark catalytic and photocatalytic methanation of CO₂.

Table II- 2. Summary of various CO₂ methanation catalysts and photocatalysts

Sample	Metal precursors	CO ₂ conversion (%)	CH ₄ selectivity (%)	T (K)	GHSV (h ⁻¹)	Stoichiometry	Flow (mL·min ⁻¹)	Ref
Hydrotalcite	Al, La, Mg, Ni	46.5; 75	98; 99	523; 573	512	H ₂ /CO ₂ /Ar=12/3/5	100	[66,67]
Hydrotalcite	Ni, Mg, Al	42-92	85; ≈100	523; 623	2,400; 40-60	H ₂ /CO ₂ =4/1	40; 200-300	[68,69]
Hydrotalcite	Fe, Mn, Ni, Al	85-94	>99	523-573	200	H ₂ /CO ₂ /Ar=4/1/5	150 NL h ⁻¹ g _{cat} ⁻¹	[70]
Ni/CeO ₂ Ni/Al ₂ O ₃ Ni/TiO ₂	Ni, Ce, Al, Ti	≈90 ≈57 ≈30	≈100 ≈97 ≈99	623	10	H ₂ /CO ₂ =4/1	100	[55]
Ni/Al ₂ O ₃ Ni-La/Al ₂ O ₃ Ni-Ce/Al ₂ O ₃	Ni, La, Ce, Ca, Ba, Mg	86 99 95	≈99	673	38.3	H ₂ /CO ₂ =4/1	280	[40]
Rh/TiO ₂	Rh, Ti	5-16	>98	623	N/A	H ₂ /CO ₂ /Ar = 6.1/1.6/2.4	250	[71][60] a, b, c
Ru/STO	Ru	89.5 in 1 h	12.6 mmol/(g·h)	423	44.6	H ₂ /CO ₂ =4/1		[72] ^d
Au/TiO ₂ K-Au/CeO ₂ Au/CeO ₂	Au, Ce, Ti	20-50 5-50 5-38	N/A	573-773	3000-6000	H ₂ /CO ₂ =4/1	N/A	[46] ^f
Ni/SiO ₂ ·Al ₂ O ₃	Ni	94.9 ^e	97.2	<423	N/A	H ₂ /CO ₂ /N ₂ =7/1.5/1.5	N/A	[73]
Rh-Ni/CeO ₂	Rh, Ni, Ce	9,8-45	100-83	573-673	5100	CH ₄ /CO ₂ /H ₂ /N ₂ =1.5/1/4/0.15	100	[74]
N10/CZ N9F1/CZ N5F5/CZ N7.5F2.5/CZ	Ni, Fe, Ce, Zr	61,5-70 45.2-58.2 24.8-32 24.8-36.8	>99 >99 10 90	573-623	21,500 mL/g·h	H ₂ /CO ₂ =4/1	50.2	[75] ^f

Sample	Metal precursors	CO ₂ conversion (%)	CH ₄ selectivity (%)	T (K)	GHSV (h ⁻¹)	Stoichiometry	Flow (mLN·min ⁻¹)	Ref
Au/SiO₂	Ni, Au, Si	9	21	723	24,000	CO ₂ /H ₂ /N ₂ = 1:4:1	24	[45]
		19 ^g	47					
		9 ^h	29					
Ni/SiO₂		42	82					
		52 ^g	86					
		45 ^h	82					
Ni-Au/SiO₂	18	90						
	34 ^g	88						
	29 ^h	78						

^a: LED light of 2.8W cm⁻² ^b: No incident light ^c: LED light of 1W cm⁻² ^d:1,080W/m² ^e: Solar simulator coupled with an AM1.5 filter ^f: 500W medium pressure mercury vapor lamp; ^g:Laser light 520 nm; ^h: Laser light 620 nm

References

- [1] M. Thema, F. Bauer, M. Sterner, Power-to-Gas: Electrolysis and methanation status review, *Renew. Sustain. Energy Rev.* 112 (2019) 775–787. <https://doi.org/10.1016/j.rser.2019.06.030>.
- [2] C. Wulf, J. Linssen, P. Zapp, Power-to-gas-concepts, demonstration, and prospects, Christina Wulf, 2018. <https://doi.org/10.1016/B978-0-12-811197-0.00009-9>.
- [3] IEA (2022), Global Hydrogen Review 2022, IEA, Paris, (n.d.). <https://www.iea.org/reports/global-hydrogen-review-2022>,.
- [4] M. Carmo, D.L. Fritz, J. Mergel, D. Stolten, A comprehensive review on PEM water electrolysis, *Int. J. Hydrogen Energy.* 38 (2013) 4901–4934. <https://doi.org/10.1016/j.ijhydene.2013.01.151>.
- [5] S. Shiva Kumar, V. Himabindu, Hydrogen production by PEM water electrolysis – A review, *Mater. Sci. Energy Technol.* 2 (2019) 442–454. <https://doi.org/10.1016/j.mset.2019.03.002>.
- [6] S. Mucci, A. Mitsos, D. Bongartz, Power-to-X processes based on PEM water electrolyzers: A review of process integration and flexible operation, *Comput. Chem. Eng.* 175 (2023) 108260. <https://doi.org/10.1016/j.compchemeng.2023.108260>.
- [7] M. Ni, M.K.H.L. Å, D.Y.C. Leung, Technological development of hydrogen production by solid oxide electrolyzer cell (SOEC), 33 (2008) 2337–2354. <https://doi.org/10.1016/j.ijhydene.2008.02.048>.

- [8] Q. Zhang, Z. Chang, M. Fu, T. Ren, X. Li, Thermal and electrochemical performance analysis of an integrated solar SOEC reactor for hydrogen production, *Appl. Therm. Eng.* 229 (2023) 120603. <https://doi.org/10.1016/j.applthermaleng.2023.120603>.
- [9] G. Min, S. Choi, J. Hong, A review of solid oxide steam-electrolysis cell systems: Thermodynamics and thermal integration, *Appl. Energy*. 328 (2022) 120145. <https://doi.org/10.1016/j.apenergy.2022.120145>.
- [10] J. Lindorfer, G. Reiter, R. Tichler, H. Steinmüller, Hydrogen fuel, fuel cells, and methane, 2018. <https://doi.org/10.1016/B978-0-12-814104-5.00014-4>.
- [11] J. Brauns, T. Turek, *Electrochimica Acta* Experimental evaluation of dynamic operating concepts for alkaline water electrolyzers powered by renewable energy, *Electrochim. Acta*. 404 (2022) 139715. <https://doi.org/10.1016/j.electacta.2021.139715>.
- [12] M. Pasichnyk, P. Stanovsky, P. Polezhaev, B. Zach, M. Šyc, M. Bobák, J.C. Jansen, M. Přebyl, J.E. Bara, K. Friess, J. Havlica, D.L. Gin, R.D. Noble, P. Izák, Membrane technology for challenging separations: Removal of CO₂, SO₂ and NO_x from flue and waste gases, *Sep. Purif. Technol.* 323 (2023) 124436. <https://doi.org/10.1016/j.seppur.2023.124436>.
- [13] L.K.G. Bhatta, S. Subramanyam, M.D. Chengala, S. Olivera, K. Venkatesh, Progress in hydrotalcite like compounds and metal-based oxides for CO₂ capture: A review, *J. Clean. Prod.* 103 (2015) 171–196. <https://doi.org/10.1016/j.jclepro.2014.12.059>.

- [14] M.R. Rahimpour, S. Mazinani, B. Vaferi, M.S. Baktash, Comparison of two different flow types on CO removal along a two-stage hydrogen permselective membrane reactor for methanol synthesis, *Appl. Energy*. 88 (2011) 41–51. <https://doi.org/10.1016/j.apenergy.2010.04.022>.
- [15] J.R. Khusnutdinova, J.A. Garg, D. Milstein, Combining Low-Pressure CO₂ Capture and Hydrogenation to Form Methanol, *ACS Catal.* 5 (2015) 2416–2422. <https://doi.org/10.1021/acscatal.5b00194>.
- [16] R. Steinberger-wilckens, B. Sampson, and Deployment d Toward Appreciating Total Owner Cost of Hydrogen Energy Technologies, Elsevier Inc., 2019. <https://doi.org/10.1016/B978-0-12-814251-6.00008-3>.
- [17] I. Agirre, E. Acha, J.F. Cambra, V.L. Barrio, Water sorption enhanced CO₂ methanation process: Optimization of reaction conditions and study of various sorbents, *Chem. Eng. Sci.* 237 (2021). <https://doi.org/10.1016/j.ces.2021.116546>.
- [18] D. Schmider, L. Maier, O. Deutschmann, Reaction Kinetics of CO and CO₂Methanation over Nickel, *Ind. Eng. Chem. Res.* 60 (2021) 5792–5805. <https://doi.org/10.1021/acs.iecr.1c00389>.
- [19] M. Ahmadi, V.G. Gomes, K. Ngian, Advanced modelling in performance optimization for reactive separation in industrial CO₂ removal, *Sep. Purif. Technol.* 63 (2008) 107–115. <https://doi.org/10.1016/j.seppur.2008.04.016>.
- [20] M. Liu, L. Zhan, Y. Wang, X. Zhao, J. Wu, D. Deng, J. Jiang, X. Zheng, Y. Lei, Achieving integrated capture and reduction of CO₂: A promising electrocatalyst,

- J. Mater. Sci. Technol. 165 (2023) 235–243.
<https://doi.org/10.1016/j.jmst.2023.06.001>.
- [21] J. Schneidewind, R. Adam, W. Baumann, R. Jackstell, M. Beller, Low-Temperature Hydrogenation of Carbon Dioxide to Methanol with a Homogeneous Cobalt Catalyst, *Angew. Chemie - Int. Ed.* 56 (2017) 1890–1893.
<https://doi.org/10.1002/anie.201609077>.
- [22] H. Sugiyama, M. Miyazaki, M. Sasase, M. Kitano, H. Hosono, Room-Temperature CO₂ Hydrogenation to Methanol over Air-Stable hcp-PdMo Intermetallic Catalyst, *J. Am. Chem. Soc.* (2022). <https://doi.org/10.1021/jacs.2c13801>.
- [23] X. Jiang, X. Nie, X. Guo, C. Song, J.G. Chen, Recent Advances in Carbon Dioxide Hydrogenation to Methanol via Heterogeneous Catalysis, *Chem. Rev.* 120 (2020) 7984–8034. <https://doi.org/10.1021/acs.chemrev.9b00723>.
- [24] S. Schemme, J.L. Breuer, M. Köller, S. Meschede, F. Walman, R.C. Samsun, R. Peters, D. Stolten, H₂-based synthetic fuels: A techno-economic comparison of alcohol, ether and hydrocarbon production, *Int. J. Hydrogen Energy.* 45 (2020) 5395–5414. <https://doi.org/10.1016/j.ijhydene.2019.05.028>.
- [25] A. Bolt, I. Dincer, M. Agelin-Chaab, Design and assessment of a new helical fixed bed type CO₂ methanation reactor, *Fuel.* 337 (2023) 127176.
<https://doi.org/10.1016/j.fuel.2022.127176>.
- [26] P. Aragüés-Aldea, A. Sanz-Martínez, P. Durán, E. Francés, J.A. Peña, J. Herguido, Improving CO₂ methanation performance by distributed feeding in a Ni-Mn catalyst fixed bed reactor, *Fuel.* 321 (2022).

- <https://doi.org/10.1016/j.fuel.2022.124075>.
- [27] M. Younas, L. Loong Kong, M.J.K. Bashir, H. Nadeem, A. Shehzad, S. Sethupathi, Recent Advancements, Fundamental Challenges, and Opportunities in Catalytic Methanation of CO₂, *Energy and Fuels*. 30 (2016) 8815–8831. <https://doi.org/10.1021/acs.energyfuels.6b01723>.
- [28] M. Hervy, J. Maistrello, L. Brito, M. Rizand, E. Basset, Y. Kara, M. Maheut, Power-to-gas: CO₂ methanation in a catalytic fluidized bed reactor at demonstration scale, experimental results and simulation, *J. CO₂ Util.* 50 (2021) 101610. <https://doi.org/10.1016/j.jcou.2021.101610>.
- [29] J. Lefebvre, N. Trudel, S. Bajohr, T. Kolb, A study on three-phase CO₂ methanation reaction kinetics in a continuous stirred-tank slurry reactor, *Fuel*. 217 (2018) 151–159. <https://doi.org/10.1016/j.fuel.2017.12.082>.
- [30] D.S. Ghosh, Visible-Light-Active Photocatalysis Nanostructured Catalyst Design, Mechanisms, and Applications, 2018. <https://doi.org/10.1002/9783527808175>.
- [31] S. Sarina, E.R. Waclawik, H. Zhu, Photocatalysis on supported gold and silver nanoparticles under ultraviolet and visible light irradiation, *Green Chem.* 15 (2013) 1814–1833. <https://doi.org/10.1039/c3gc40450a>.
- [32] P. Chemistry, C. Physics, *Physical Chemistry Chemical Physics*, 16 (2014). <https://doi.org/10.1039/c3cp54411g>.
- [33] E. Commission, No Title, Brussel, 16.3.2023 COM(2023) 160 Final. (2023) 94. <https://eur-lex.europa.eu/legal-content/EN/TXT/HTML/?uri=CELEX:52023PC0160>.

- [34] “European Commission, Study on the Critical Raw Materials for the EU 2023 – Final Report,” (n.d.).
- [35] L. Falbo, C.G. Visconti, L. Lietti, J. Szanyi, The effect of CO on CO₂ methanation over Ru/Al₂O₃ catalysts: a combined steady-state reactivity and transient DRIFT spectroscopy study, *Appl. Catal. B Environ.* 256 (2019) 117791. <https://doi.org/10.1016/j.apcatb.2019.117791>.
- [36] S. Siegel, Ruthenium Catalysts, *Encycl. Reagents Org. Synth.* 1 (2001). <https://doi.org/10.1002/047084289x.rr007>.
- [37] M. Bailera, P. Lisbona, B. Peña, A. Alarcón, J. Guilera, J. Perpiñán, L.M. Romeo, Synthetic natural gas production in a 1 kW reactor using Ni–Ce/Al₂O₃ and Ru–Ce/Al₂O₃: Kinetics, catalyst degradation and process design, *Energy*. 256 (2022). <https://doi.org/10.1016/j.energy.2022.124720>.
- [38] W. Gac, W. Zawadzki, G. Słowik, A. Sienkiewicz, A. Kierys, Nickel catalysts supported on silica microspheres for CO₂ methanation, *Microporous Mesoporous Mater.* 272 (2018) 79–91. <https://doi.org/10.1016/j.micromeso.2018.06.022>.
- [39] A. Cárdenas-Arenas, A. Quindimil, A. Davó-Quiñonero, E. Bailón-García, D. Lozano-Castelló, U. De-La-Torre, B. Pereda-Ayo, J.A. González-Marcos, J.R. González-Velasco, A. Bueno-López, Isotopic and in situ DRIFTS study of the CO₂ methanation mechanism using Ni/CeO₂ and Ni/Al₂O₃ catalysts, *Appl. Catal. B Environ.* 265 (2020). <https://doi.org/10.1016/j.apcatb.2019.118538>.
- [40] D. Méndez-Mateos, V.L. Barrio, J.M. Requies, J.F. Cambra, A study of

- deactivation by H₂S and regeneration of a Ni catalyst supported on Al₂O₃, during methanation of CO₂. Effect of the promoters Co, Cr, Fe and Mo, *RSC Adv.* 10 (2020) 16551–16564. <https://doi.org/10.1039/d0ra00882f>.
- [41] L. Xu, X. Lian, M. Chen, Y. Cui, F. Wang, W. Li, B. Huang, CO₂ methanation over Co–Ni bimetal-doped ordered mesoporous Al₂O₃ catalysts with enhanced low-temperature activities, *Int. J. Hydrogen Energy.* 43 (2018) 17172–17184. <https://doi.org/10.1016/j.ijhydene.2018.07.106>.
- [42] C. Liang, H. Tian, G. Gao, S. Zhang, Q. Liu, D. Dong, X. Hu, Methanation of CO₂ over alumina supported nickel or cobalt catalysts: Effects of the coordination between metal and support on formation of the reaction intermediates, *Int. J. Hydrogen Energy.* 45 (2020) 531–543. <https://doi.org/10.1016/j.ijhydene.2019.10.195>.
- [43] J. Kirchner, J.K. Anolleck, H. Lösch, S. Kureti, Methanation of CO₂ on iron based catalysts, *Appl. Catal. B Environ.* 223 (2018) 47–59. <https://doi.org/10.1016/j.apcatb.2017.06.025>.
- [44] I. García-García, E.C. Lovell, R.J. Wong, V.L. Barrio, J. Scott, J.F. Cambra, R. Amal, Silver-Based Plasmonic Catalysts for Carbon Dioxide Reduction, *ACS Sustain. Chem. Eng.* 8 (2020) 1879–1887. <https://doi.org/10.1021/acssuschemeng.9b06146>.
- [45] J.N.G. Stanley, I. García-García, T. Perfrement, E.C. Lovell, T.W. Schmidt, J. Scott, R. Amal, Plasmonic effects on CO₂ reduction over bimetallic Ni-Au catalysts, *Chem. Eng. Sci.* 194 (2019) 94–104. <https://doi.org/10.1016/j.ces.2018.04.003>.

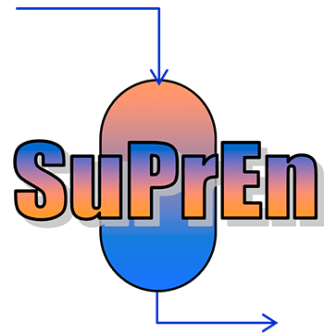
- [46] G. Halasi, A. Gazsi, T. Bánsági, F. Solymosi, Catalytic and photocatalytic reactions of H₂ + CO₂ on supported Au catalysts, *Appl. Catal. A Gen.* 506 (2015) 85–90. <https://doi.org/10.1016/j.apcata.2015.08.035>.
- [47] E.M. Mendoza-Núñez, J.C. Fierro-Gonzalez, T.A. Zepeda, A. Solis-Garcia, Effect of platinum addition on the reaction mechanism of the CO₂ methanation catalyzed by ZrO₂-supported Rh, *Mol. Catal.* 533 (2022). <https://doi.org/10.1016/j.mcat.2022.112801>.
- [48] J. Gao, C. Jia, J. Li, M. Zhang, F. Gu, G. Xu, Z. Zhong, F. Su, Ni/Al₂O₃ catalysts for CO methanation: Effect of Al₂O₃ supports calcined at different temperatures, *J. Energy Chem.* 22 (2013) 919–927. [https://doi.org/10.1016/S2095-4956\(14\)60273-4](https://doi.org/10.1016/S2095-4956(14)60273-4).
- [49] T.A. Le, J.K. Kang, E.D. Park, Active Ni/SiO₂ catalysts with high Ni content for benzene hydrogenation and CO methanation, *Appl. Catal. A Gen.* 581 (2019) 67–73. <https://doi.org/10.1016/j.apcata.2019.05.020>.
- [50] T.A. Le, J.K. Kang, E.D. Park, CO and CO₂ Methanation Over Ni/SiC and Ni/SiO₂ Catalysts, *Top. Catal.* 61 (2018) 1537–1544. <https://doi.org/10.1007/s11244-018-0965-7>.
- [51] X. Yan, Y. Liu, B. Zhao, Z. Wang, Y. Wang, C.J. Liu, Methanation over Ni/SiO₂: Effect of the catalyst preparation methodologies, *Int. J. Hydrogen Energy.* 38 (2013) 2283–2291. <https://doi.org/10.1016/j.ijhydene.2012.12.024>.
- [52] M. Romero-Sáez, A.B. Dongil, N. Benito, R. Espinoza-González, N. Escalona, F. Gracia, CO₂ methanation over nickel-ZrO₂ catalyst supported on carbon

- nanotubes: A comparison between two impregnation strategies, *Appl. Catal. B Environ.* 237 (2018) 817–825. <https://doi.org/10.1016/j.apcatb.2018.06.045>.
- [53] Y. Zhan, Y. Wang, D. Gu, C. Chen, L. Jiang, K. Takehira, Ni/Al₂O₃-ZrO₂ catalyst for CO₂ methanation: The role of γ -(Al, Zr)₂O₃ formation, *Appl. Surf. Sci.* 459 (2018) 74–79. <https://doi.org/10.1016/j.apsusc.2018.07.206>.
- [54] C. Fukuhara, K. Hayakawa, Y. Suzuki, W. Kawasaki, R. Watanabe, A novel nickel-based structured catalyst for CO₂ methanation: A honeycomb-type Ni/CeO₂ catalyst to transform greenhouse gas into useful resources, *Appl. Catal. A Gen.* 532 (2017) 12–18. <https://doi.org/10.1016/j.apcata.2016.11.036>.
- [55] S. Tada, T. Shimizu, H. Kameyama, T. Haneda, R. Kikuchi, Ni/CeO₂ catalysts with high CO₂ methanation activity and high CH₄ selectivity at low temperatures, *Int. J. Hydrogen Energy.* 37 (2012) 5527–5531. <https://doi.org/10.1016/j.ijhydene.2011.12.122>.
- [56] K. Stangeland, D. Kalai, H. Li, Z. Yu, CO₂ Methanation: The Effect of Catalysts and Reaction Conditions, *Energy Procedia.* 105 (2017) 2022–2027. <https://doi.org/10.1016/j.egypro.2017.03.577>.
- [57] N.M. Martin, P. Velin, M. Skoglundh, M. Bauer, P.A. Carlsson, Catalytic hydrogenation of CO₂ to methane over supported Pd, Rh and Ni catalysts, *Catal. Sci. Technol.* 7 (2017) 1086–1094. <https://doi.org/10.1039/c6cy02536f>.
- [58] M.C. Bacariza, I. Graça, J.M. Lopes, C. Henriques, Enhanced activity of CO₂ hydrogenation to CH₄ over Ni based zeolites through the optimization of the Si/Al ratio, *Microporous Mesoporous Mater.* 267 (2018) 9–19.

- <https://doi.org/10.1016/j.micromeso.2018.03.010>.
- [59] M.C. Bacariza, M. Maleval, I. Graça, J.M. Lopes, C. Henriques, Power-to-methane over Ni/zeolites: Influence of the framework type, *Microporous Mesoporous Mater.* 274 (2019) 102–112. <https://doi.org/10.1016/j.micromeso.2018.07.037>.
- [60] X. Zhang, X. Li, M.E. Reish, D. Zhang, N.Q. Su, Y. Gutiérrez, F. Moreno, W. Yang, H.O. Everitt, J. Liu, Plasmon-Enhanced Catalysis: Distinguishing Thermal and Nonthermal Effects, *Nano Lett.* 18 (2018) 1714–1723. <https://doi.org/10.1021/acs.nanolett.7b04776>.
- [61] M.A. Serrer, A. Gaur, J. Jelic, S. Weber, C. Fritsch, A.H. Clark, E. Saraçi, F. Studt, J.D. Grunwaldt, Structural dynamics in Ni-Fe catalysts during CO₂ methanation—role of iron oxide clusters, *Catal. Sci. Technol.* 10 (2020) 7542–7554. <https://doi.org/10.1039/d0cy01396j>.
- [62] P. Summa, K. Świrk, Y. Wang, B. Samojeden, M. Rønning, C. Hu, M. Motak, P. Da Costa, Effect of cobalt promotion on hydrotalcite-derived nickel catalyst for CO₂ methanation, *Appl. Mater. Today.* 25 (2021) 101211. <https://doi.org/10.1016/j.apmt.2021.101211>.
- [63] X. Wang, T. Zhen, C. Yu, Application of Ni–Al-hydrotalcite-derived catalyst modified with Fe or Mg in CO₂ methanation, *Appl. Petrochemical Res.* 6 (2016) 217–223. <https://doi.org/10.1007/s13203-016-0154-1>.
- [64] L. Yin, X. Chen, M. Sun, B. Zhao, J. Chen, Q. Zhang, P. Ning, Insight into the role of Fe on catalytic performance over the hydrotalcite-derived Ni-based catalysts for CO₂ methanation reaction, *Int. J. Hydrogen Energy.* 47 (2022) 7139–7149.

- <https://doi.org/10.1016/j.ijhydene.2021.12.057>.
- [65] C. Italiano, R. Balzarotti, A. Vita, S. Latorrata, C. Fabiano, L. Pino, C. Cristiani, Preparation of structured catalysts with Ni and Ni–Rh/CeO₂ catalytic layers for syngas production by biogas reforming processes, *Catal. Today*. 273 (2016) 3–11. <https://doi.org/10.1016/j.cattod.2016.01.037>.
- [66] D. Wierzbicki, R. Debek, M. Motak, T. Grzybek, M.E. Gálvez, P. Da Costa, Novel Ni-La-hydrotalcite derived catalysts for CO₂ methanation, *Catal. Commun.* 83 (2016) 5–8. <https://doi.org/10.1016/j.catcom.2016.04.021>.
- [67] D. Wierzbicki, M. Motak, T. Grzybek, M.E. Gálvez, P. Da Costa, The influence of lanthanum incorporation method on the performance of nickel-containing hydrotalcite-derived catalysts in CO₂ methanation reaction, *Catal. Today*. 307 (2018) 205–211. <https://doi.org/10.1016/j.cattod.2017.04.020>.
- [68] P. Marocco, E.A. Morosanu, E. Giglio, D. Ferrero, C. Mebrahtu, A. Lanzini, S. Abate, S. Bensaid, S. Perathoner, M. Santarelli, R. Pirone, G. Centi, CO₂ methanation over Ni/Al hydrotalcite-derived catalyst: Experimental characterization and kinetic study, *Fuel*. 225 (2018) 230–242. <https://doi.org/10.1016/j.fuel.2018.03.137>.
- [69] X. Guo, D. Gao, H. He, A. Traitangwong, M. Gong, V. Meeyoo, Z. Peng, C. Li, Promotion of CO₂ methanation at low temperature over hydrotalcite-derived catalysts-effect of the tunable metal species and basicity, *Int. J. Hydrogen Energy*. 46 (2020) 518–530. <https://doi.org/10.1016/j.ijhydene.2020.09.193>.
- [70] T. Burger, F. Koschany, O. Thomys, K. Köhler, O. Hinrichsen, CO₂ methanation

- over Fe- and Mn-promoted co-precipitated Ni-Al catalysts: Synthesis, characterization and catalysis study, *Appl. Catal. A Gen.* 558 (2018) 44–54. <https://doi.org/10.1016/j.apcata.2018.03.021>.
- [71] X. Zhang, X. Li, D. Zhang, N.Q. Su, W. Yang, H.O. Everitt, J. Liu, Product selectivity in plasmonic photocatalysis for carbon dioxide hydrogenation, *Nat. Commun.* 8 (2017) 1–9. <https://doi.org/10.1038/ncomms14542>.
- [72] D. Mateo, J. Albero, H. García, Titanium-Perovskite-Supported RuO₂ Nanoparticles for Photocatalytic CO₂ Methanation, *Joule.* 3 (2019) 1949–1962. <https://doi.org/10.1016/j.joule.2019.06.001>.
- [73] F. Sastre, A. V. Puga, L. Liu, A. Corma, H. García, Complete photocatalytic reduction of CO₂ to methane by H₂ under solar light irradiation, *J. Am. Chem. Soc.* 136 (2014) 6798–6801. <https://doi.org/10.1021/ja500924t>.
- [74] R. Balzarotti, G. Drago Ferrante, C. Italiano, M. Laganà, L.F. Francis, A. Vita, C. Cristiani, L. Pino, RhNi/CeO₂ catalytic activation of alumina open cell foams by dip-spin coating for the CO₂ methanation of biogas, *Surf. Coatings Technol.* 441 (2022). <https://doi.org/10.1016/j.surfcoat.2022.128563>.
- [75] G. De Piano, J.J.A. Gamboa, A.M. Condó, S. Bengió, F.C. Gennari, Bimetallic Ni-Fe catalysts for methanation of CO₂: Effect of the support nature and reducibility, *Appl. Catal. A Gen.* 634 (2022). <https://doi.org/10.1016/j.apcata.2022.118540>.



**Rafael Canales Larrazabal
Bilbao, 2023**



Universidad
del País Vasco

Euskal Herriko
Unibertsitatea

MDe

Master eta Doktorego Eskola
Escuela de Máster y Doctorado
Master and Doctoral School

CHAPTER III

OBJECTIVES

CHAPTER III. OBJECTIVES

The main objective of this PhD thesis is to address several challenges related to methane generation through a photocatalytic process using CO₂ and H₂ derived from renewable resources. In order to conduct experimental activities, a dedicated commercial photocatalytic reactor was employed for this project.

One of the key focuses is on exploring the plasmonic effect of noble and non-noble metals, which were deposited on various **supports** such as **alumina**, **titania** and **hydrotalcite-derived materials**. The aim is to compare their catalytic activity in the methane generation process. Advanced techniques were utilized to prepare these systems, incorporating metals like **gold and nickel** as active catalysts, along with other other metals such as **ceria**, **cobalt**, **iron and molybdenum**. This approach helps to gain insights into the characteristics of each element and their role in enhancing the Sabatier reaction, which is involved in the methane generation process.

- ✓ Initially, the influence of gold deposition on commercial TiO₂ was investigated due to the plasmonic effect enhancing the photocatalytic reduction of CO₂ to CH₄ under solar irradiation.
- ✓ The influence of TiO₂ and γ-Al₂O₃ as supports for a fixed Ni content was investigated.
- ✓ The influence of Ni content variation on γ-Al₂O₃ was analyzed following a well-known methodology.

✓ In the case of HTCs, with Ce as a trivalent metal (Ce_2O_3), an amount of Al was replaced by the addition of Ce in order to maintain the same concentration of trivalent metals. Ce optimization was investigated to improve reaction activity, especially at low temperature.

✓ Considering Co as divalent metal (CoO), an amount of Ni was replaced by the addition of Co in order to maintain the same active metal content as Co is active to the Sabatier reaction. Indeed comparison of their monometallic activity (Ni and Co) with the Ni-Co interaction will be studied.

✓ With Fe as a trivalent metal (Fe_2O_3), an amount of Al was replaced by the addition of Fe in order to maintain the same concentration of trivalent metals. The role of Fe as a support and as an active metal has not been investigated by comparing its catalytic and photocatalytic influence, previously.

✓ Finally, two different Mo contents were impregnated to a previously prepared Ni-HTC in order to analyze the influence of this metal on the reaction since it is considered to be active in visible light.

Furthermore, the research takes into account the Sustainable Development Goals (SDGs) and the impact associated with the use of critical raw materials listed in Chapter II.7. By investigating alternative catalysts and exploring renewable resources for methane generation, the aim is to contribute to sustainable and environmentally friendly processes that align with the SDGs. This research also considers the reduction of reliance on critical raw materials, which are often associated with environmental concerns and geopolitical challenges.

Overall, this PhD thesis strives to develop a photo-catalytic process for methane generation, employing novel catalysts and renewable resources, while considering the sustainability aspects outlined by the SDGs and minimizing the use of critical raw materials.

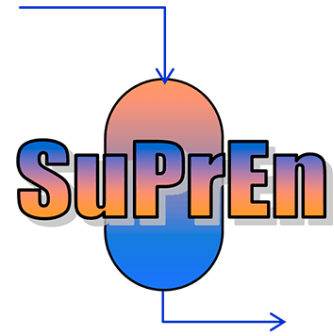
Finally, the objective of washcoating of HTC-Ce and Katalco 57-4Q was to scale-up catalysts in order to ensure the efficient and uniform application of the catalytic material onto a larger surface area or substrate. The following aspects will be analyzed and improved in order to finally test these two materials in a fixed bed reactor, optimizing also the different spatial velocities and how these affect both the activity and the effect stability of the material after the tests. The main goals of the scale up through the washcoating are as follows:

- ✓ Increased catalytic efficiency: The primary objective is to maintain or enhance the catalytic efficiency of the coated catalyst. By uniformly distributing the catalytic material onto the larger substrate, the active surface area available for catalysis is maximized. This ensures that the catalytic reaction can proceed effectively and with high conversion rates.

- ✓ Consistency and reproducibility: Scaling up the washcoating process aims to achieve consistent and reproducible results across multiple coated substrates. This involves optimizing the process parameters, such as coating thickness, deposition technique, and drying conditions, to ensure uniform coating distribution and composition. Consistency and reproducibility are crucial for industrial applications, as they allow for reliable and predictable catalytic performance.

✓ Adhesion and stability: The washcoating process should ensure strong adhesion of the catalytic material to the substrate to prevent its detachment or degradation during operation. Proper substrate preparation, choice of binder materials, and curing conditions are important factors that will be analyzed in achieving good adhesion and long-term stability of the coated catalyst.

By achieving these objectives, the washcoating process for scale-up will enable the successful transition from laboratory-scale catalyst preparation to large-scale industrial production, ensuring the desired catalytic performance, consistency, and cost-efficiency.



Rafael Canales Larrazabal
Bilbao, 2023



Universidad
del País Vasco

Euskal Herriko
Unibertsitatea



Master eta Doktorego Eskola
Escuela de Máster y Doctorado
Master and Doctoral School

CHAPTER IV

EXPERIMENTAL SECTION

CHAPTER IV. EXPERIMENTAL

IV.1. Catalyst Preparation

Three different preparation techniques were employed depending on the type of metal-support interaction:

Firstly, monometallic Ni/Al₂O₃ catalysts were prepared by incipient wetness impregnation method. The support prior to its synthesis, it was necessary to determine the pore volume in order to add three times more milli-Q water filling all pores in contact with the dissolved metal. The pH of the solution is an important aspect due to the ionic adsorption (Van der Waals and electrostatic) forces involved between nickel and alumina. The pH at which these charges are neutralized is called isoelectric point pH_{iep} .

A homogeneous mixture of the solution of alumina and nickel nitrate after mixing was added into a rotavapor (Heidolph Laborota 4000), equipped with a vacuum pump for reducing the temperature needed to evaporate water and extract it. The flask was submerged at 338 K under a rotation of 200 rpm [1].

After evaporation of the aqueous solution, the solid part was dried overnight at 373 K. Afterwards, the sample was ground for a homogeneous calcination at 673 K (5 K/min) to obtain a more homogeneous particle size calcination. For reaction conditions, catalysts particles were pressed at 8 tonnes and sieved to a particle size of 0.42mm < particle size < 0.50 mm.

The materials employed for synthesizing catalysts for 13Ni/Al₂O₃ and 25Ni/Al₂O₃ were the following ones :

- $\text{Ni}(\text{NO}_3)_2 \cdot 6\text{H}_2\text{O}$ (Sigma-Aldrich; Ref:203874)
- $\gamma\text{-Al}_2\text{O}_3$ (Alfa Aesar; Ref:43832)
- Ammonia 25 % (as NH_3) (Panreac-121129)
- Milli-Q water

Two **Monometallic Au/TiO₂** catalysts were prepared by two different methods with different gold loadings. First technique employed for 2Au/TiO₂ catalyst was prepared by anionic-adsorption method [2]. 140 mL of $\text{HAuCl}_4 \cdot 3\text{H}_2\text{O}$ ($4.2 \cdot 10^{-3}$ M) and 6g of TiO₂ were dissolved at 363 K and 500 rpm of continuous stirring. The pH of the solution was fixed at 4.7 after the addition of 0.1M HCl. After 15 min of stirring, HAuCl_4 /sodium citrate ratio of 1:9 was added to the solution. Finally, the suspension was cooled with an ice bath. The sample was filtered off and washed for the elimination of ions dissolved and dried overnight at 373 K. Finally, the solid was calcined at 573 K.

Second technique employed for 4Au/TiO₂ catalyst was prepared by deposition-precipitation method [3]. 5g of TiO₂ and 250 mL of $4.4 \cdot 10^{-3}$ M of $\text{HAuCl}_4 \cdot 3\text{H}_2\text{O}$ were dissolved in a beaker. The operational pH was fixed at 8 by the addition of 0.1M Na_2CO_3 at 363 K and 500 rpm of continuous stirring. The sample was carefully washed with distilled water to remove the ions dissolved in a centrifuge during 30 minutes at 4000 rpm. Finally, the solid was dried overnight and calcined at 573 K.

Monometallic 13Ni/TiO₂ catalyst was prepared by deposition-precipitation technique [4]. Initially, 8g of pre-calcined TiO₂ at 773 K to increase the anatase phase content of titania, which has been studied to have better photocatalytic properties.

A nickel nitrate salt/Glycerol molar ratio of 1:2 was added to a 200 mL distilled water solution. Subsequently, to the previous process, a 0.5 M NaOH solution was added

dropwise until pH 12. The resulting suspension obtained was stirred at 343 K. The product was filtered off, washed thoroughly with distilled water and dried overnight at 373 K. Finally, the sample was calcined at 573 K (5 K/min).

The materials employed for synthesizing catalysts for $^{13}\text{Ni}/\text{TiO}_2$ were the following ones :

- TiO_2 (Sigma-Aldrich; REF:718467)
- Glycerol (Panreac; REF:151339)
- $\text{Ni}(\text{NO}_3)_2 \cdot 6\text{H}_2\text{O}$ (Sigma-Aldrich; Ref:203874)
- NaOH (Honeywell; Ref: 011-002-00-6)

Hydrotalcite-derived materials were prepared by co-precipitation technique at a constant pH of 10 replacing divalent (M^{2+}) or trivalent metals (M^{3+}) [5]. The molarity was fixed maintaining a molar ratio of $\text{M}^{2+}/\text{M}^{3+}$ equal to 3. This ratio is also seen in natural hydrotalcite : $\text{Mg}_6\text{Al}_2\text{CO}_3(\text{OH})_{16} \cdot 4\text{H}_2\text{O}$ and under this premise, the ratio remained unchanged for all hydrotalcites synthesized. The basic pH was obtained by mixing a precipitant solution of 2M of NaOH and 0.125M of Na_2CO_3 which was subsequently introduced into a burette. This mixed solution was dropped wisely in a flask containing 1M of metal salts diluted under continuous stirring (500 rpm) until the desired pH was stabilized. The precipitate sample was fulfilled at room temperature for and aged for 24 h. Subsequently, the slurry was filtered under pressure, washed thoroughly with distilled water and dried at 373 K. Finally, the dried solid was calcined at 773 K (5 K/min) during 4 h with the sample particle size previous catalysts. The process from the hydrotalcite structure as synthesized and finally, the structure after

calcination is observed in Figure IV- 1. The nominal weight content of the four different HTC's are listed in Table IV.1-4).

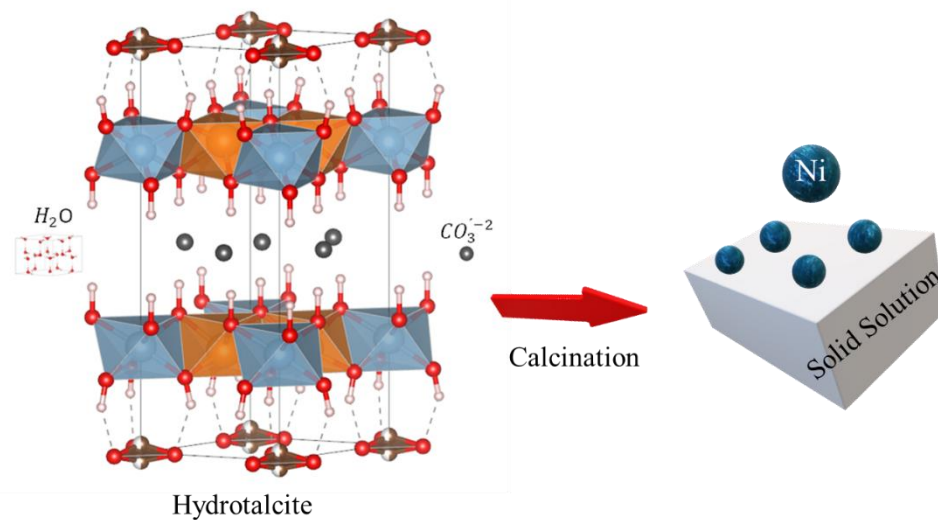


Figure IV- 1. Hydrotalcite structural changes during synthesis and calcination process

The materials employed for synthesizing catalysts for hydrotalcite-derived materials were the following ones :

- $Ni(NO_3)_2 \cdot 6H_2O$ (Sigma-Aldrich; Ref:203874)
- $Ce(NO_3)_3 \cdot 6H_2O$ (Sigma-Aldrich; Ref: 202991)
- $Mg(NO_3)_2 \cdot 6H_2O$ (Honeywell; Ref:237175)
- $Al(NO_3)_3 \cdot 9H_2O$ (Labkem; Ref: ALNA-09A)
- $Co(NO_3)_2 \cdot 6H_2O$ (Alfa Aesar; Ref: 36418)
- $Fe(NO_3)_3 \cdot 9H_2O$ (Labkem; Ref:IRNA-09A)
- Sodium Carbonate monohydrate (Panreac; Ref: 142032.1211)
- NaOH (Honeywell; Ref: 011-002-00-6)
- $(NH_4)_6Mo_7O_{24} \cdot 4H_2O$ (Merck;Ref: 101181)

Table IV- 1. The nominal content of the HTC-Ce

	Metal content (wt. %)			
	Calcination 723 K			
	Ni	Ce	Mg	Al
HTC 1	27	-	50	23
HTC 2	26	4	48	21
HTC 3	25	11	46	18
HTC 4	23	18	43	16

Table IV- 2. The nominal content of the HTC-Co

	Metal content (wt. %)			
	Calcination 773 K			
	Ni	Co	Mg	Al
27Co	-	27	50	23
8Co-19Ni	8	19	50	23
6Co-21Ni	21	6	50	23

Table IV- 3. The nominal content of the HTC-Fe

	Metal content (wt. %)			
	Calcination 773 K			
	Ni	Fe	Mg	Al
26Fe-25Ni	23	27	43	7
16Fe-25Ni	25	15	46	13
6Fe-25Ni	26	6	49	19

Finally, two molybdenum hydrotalcite were synthesized via wetness incipient method.

Table IV- 4. The nominal content of the HTC-Mo

Metal content (wt. %)				
Calcination 773 K				
	Ni	Mo	Mg	Al
2Mo	27	2	49	22
6Mo	26	6	47	21

IV.2. Catalyst characterization for monometallic and HTC materials

IV.2.1. N₂ Adsorption-Desorption Isotherms

The textural properties of the calcined samples were analysed using N₂ physical adsorption–desorption isotherms at 77 K using initially a Quantachrome Autosorb 1C-TCD and finally a Quantachrome Autosorb IQ analyser. Prior to sample analysis, the catalysts were degassed at 373 K for 2 h followed by heating to 573 K for 8 h. The obtained isotherms were used to extract the Brunauer–Emmett–Teller (BET) surface area, pore volume, and average pore diameter with Barrett-Joyner-Halenda (BJH) method.

IV.2.2. ICP-OES

Inductively coupled plasma optical emission spectroscopy (ICP-OES) was used to analyse the metal contents in the samples. The calcined catalysts were first digested in aqua regia (HCl: HNO₃=3:1) using ETHOS 1, a milestone microwave digestion system, and then analysed using a PerkinElmer Optima 3300DV ICP-OES system. The acid solution was diluted in distilled water due to the 2% of acidity concentration needed for analysis. Additionally, different patrons containing known amounts of each metal are measured to obtain a calibration curve and compare with catalysts elemental

composition.

IV.2.3. H₂-TPR

The reducibility of the samples was evaluated by temperature-programmed reduction with hydrogen (H₂-TPR) using an AutoChem II Instrument. The calcined catalysts were pre-treated in situ by heating the samples to 473 K under He to desorb physisorbed impurities. The samples were then cooled to 303 K and heated to 1193 K at a rate of 10 K/min in a flow of reducing gas (5% v/v H₂ diluted in Ar). Monometallic catalysts supported on Al₂O₃/TiO₂ were heated to a lower temperature (923 K) due the catalysts reducibility nature of the active species.

IV.2.4. CO₂-TPD

Temperature-programmed desorption with carbon dioxide (CO₂-TPD) was used to analyse the acidic and basis site strength of the catalyst using an AutoChem II instrument. The sample was firstly degassed under He at 573 K for 1 h and then cooled to 353 K prior to adsorption of 30 mL_N/min CO₂ (5% v/v CO₂ diluted in He) during 1 h. After CO₂ adsorption, the sample was treated with He (40 mL_N/min) for 30 min to remove physically adsorbed CO₂ from the surface. The desorption curves were recorded and monitored by the TCD at a heating rate of 10 K/min from 353 to 873 K under a He flow (15 mL_N/min).

IV.2.5. XRD

X-ray diffraction (XRD) was used to observe the crystal phases of the calcined catalysts. XRD patterns were obtained using a Seifert XRD 3000 diffractometer equipped with a PW 2200 Bragg–Brentano $\theta/2\theta$ goniometer, bent graphite monochromator, and automatic slit, using Cu K radiation (0.15418 nm) and 0.028° steps for scanning. The crystalline structures of the samples were determined using a PANalytical X'PERT PRO diffractometer. Preceding the analysis, different patterns were investigated.

IV.2.6. UV-Vis-DRS

UV–visible diffuse reflectance spectroscopy (UV–vis DRS) of the powdered samples was performed using a Shimadzu UV-2100 spectrophotometer, and the results were expressed as a Kubelka–Munk function between 200 and 800 nm. The adsorption peaks obtained were correlated with the metal charge transfer transition, metal content, and particle size, among other possible analyses.

IV.2.7. XPS

X-ray photoelectron spectroscopy (XPS) was used to determine the elemental composition of the surface regions of the catalysts of the reduced samples performed in a SPECS system (Berlin, Germany) equipped with a Phoibos 150 1D-DLD analyser and a monochromatic Al $K\alpha$ radiation source (1486.6 eV). Spectra were fitted using CasaXPS software which models Gauss-Lorentzian contributions, after background subtraction (Shirley). Concentrations were calculated by correcting the values with relative atomic sensitivity factors (Scofield).

IV.2.8. H₂-Chemisorption

H₂ chemisorption technique was employed to determine metallic dispersion of the reduced catalysts. Performed in the same instrument as CO₂-TPD and H₂-TPR, the samples were firstly degassed under Ar at 573 K for 1 h and then heated to according to the reduction temperature conditions of each catalyst using (5% v/v H₂ diluted in Ar) during 1h and returning to ambient temperature. After 50 mL_N/min of Ar, for 15 min at the same temperature for desorbing impurities. The dispersion was determined by using H₂ pulses and their consumption were measured using the TCD.

IV.2.9. STEM-EDS

Scanning transmission electron microscopy–energy dispersive X-ray spectroscopy (STEM–EDS) was performed using a TECNAI G2 20 TWIN transmission electron microscope at 200 kV equipped with an EDS system (EDAX). Elemental maps of the samples were obtained to calculate the mean particle size and study the morphology of the catalysts. The samples analysed were the used ones after experimental reactions.

IV.3. Wash-coating for CO₂ methanation

In this thesis, different studies were carried out for the impregnation of two catalysts: Ce-HTC 4 and a commercial catalyst (Katalco 57 4Q) on three open alumina foam cells with different cell densities: 20-30-40 pores per inch (PPI) supplied by Lanik S.r.o.

IV.3.1. Catalyst preparation

The catalytic activation of alumina foams through via wash-coating technique was based on a methodology improved by CNR-ITAE [6]. Firstly, a homogeneous solution of

7.5g of distilled water, 0.34g of PVA (Sigma Aldrich:363081) and 9.5g of glycerol (VWR:24386) solution was mixed at 358 K. 5g of catalyst was ball milled to powder due to impact of the particle size on viscosity and added into the totally dissolved solution. The resulting slurry was stirred and finally ball-milled with ZrO_2 sphere for 24 h at 300 rpm [7]. The obtained slurry was sonicated for 30 min to reduce foaming with ethanol addition. Moreover, the pure open cell foams were sonicated in a bath with acetone to superficially clean the alumina.

Multiple dip-spin coating immersions of the alumina foam structures with into the slurry were done to obtain the required amount of coating mass. In each step coating, the foam impregnated was flash dried at 573 K until the desire catalyst loading (g/cm^3) was obtained in order to control weigh evolution, as shown in Figure IV- 2.

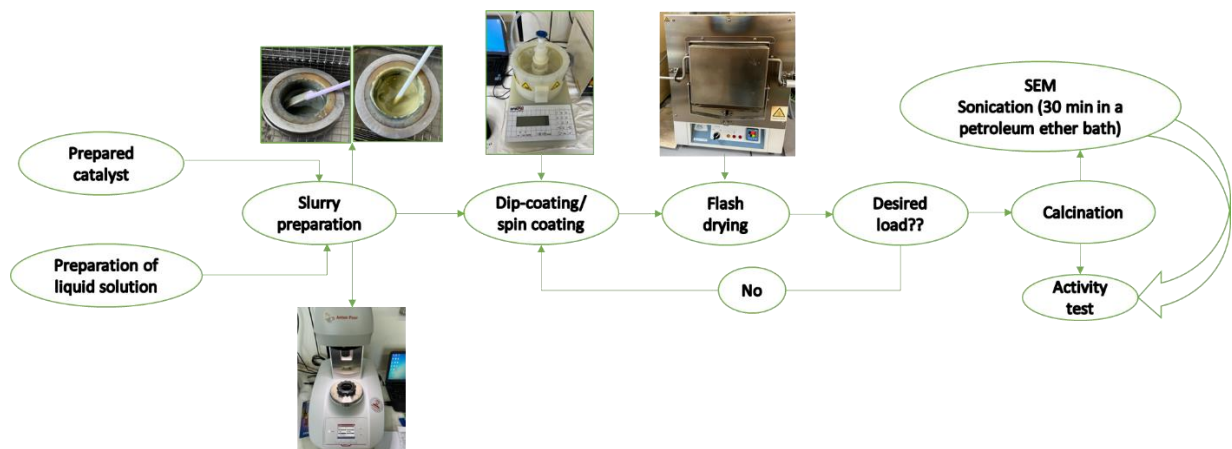
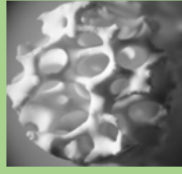
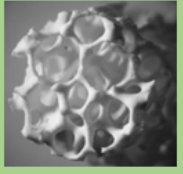
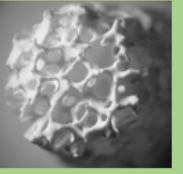


Figure IV- 2. Summary of wash-coating procedure and image

The objective was to fix the optimum process properties by varying three different steps for wash-coating process in terms of average thickness analyzed by SEM images and coating adhesion by sonication treatment:

Table IV- 5. Characteristics of the open cell foams used

	F20	F30	F40
Structured substrate			
Pore per inch, ppi	20	30	40
Diameter, ϕ - Length, L (mm)	"10-15"	"10-15"	"10-15"
Hole area, A (mm ²)	2,88	1,55	0,92
Average pore diameter, d_p (mm)	1,92	1,4	1,08
Average strut thickness, t_s (mm)	0,51	0,41	0,33
Face diameter, d_f (mm)	2,42	1,81	1,41
Relative density, ρ_r	0,11	0,13	0,14
Voidage, ε	0,89	0,87	0,86
Bed porosity, V_p (%)	88,3	85,1	83,6
Geometric surface area, GSA (m ² ·m ⁻³)	669	967	1273
Exposed surface area, SA_{OCF} (mm ²)	788	1138	1500

1. Firstly, the influence of spinning rate variation at **500, 1000 and 2000 rpm** fixing the rotation time to 20 s and a catalyst loading of 0.1 g/cm³ on 30 PPI open cell foam was the objective for further spinning rate in order to fix. During diPPInG process, the foam was immersed for 10 s to ensure that the entire surface was in contact with the slurry. Subsequently, the coated samples were flash dried for 6 min at 623K in a sealed oven and measured the weight after each dip-spin coating process. This dip-spin process was repeated until the desired load was obtained. Finally, the sample was calcined at 773K for 4 h (5 K/min).
2. Once the spin speed velocity was fixed (point 1), the variation of catalyst loading on the support was analyzed (0.1-0.2-0.3 g/cm³). The procedure was the same as Point 1.

3. After analyzing both the appropriate rotational speed (Point 1) and the catalyst loading on the support (Point 2), the variation of the support PPI was analyzed. (20, 30 and 40).



Figure IV- 3. Left) Rheological properties analyzer. Right) Spin-coater equipment

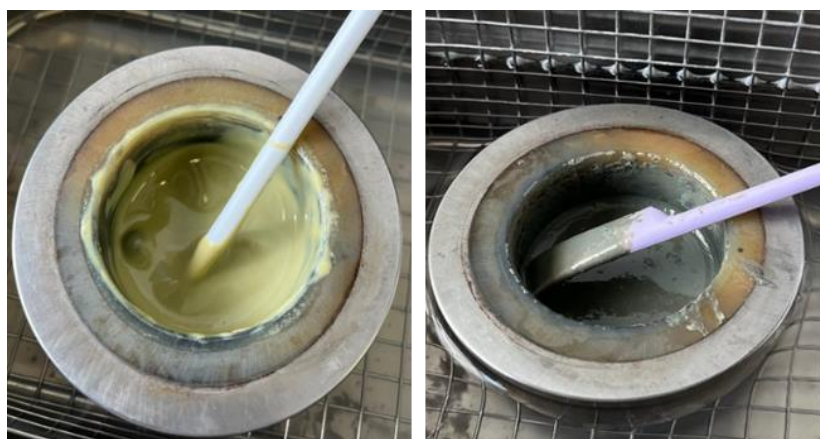


Figure IV- 4. Slurry after ball-milling and sonication. Left: Ce-Hydrotalcite. Right: Katalco.

For the activity tests, Sabatier Reaction was carried out in a continuous-flow quartz reactor (1 cm inner diameter; 25 cm length) inserted in a tubular furnace with 3 thermocouples for temperature control (inlet-middle-outlet contact). The structured catalysts were loaded in the middle covered with quartz wool to ensure a catalyst-reactor full contact. The composition of the gas phase products was determined using an on-line gas chromatograph (Agilent 6890 Plus) equipped with TCD and FID.

IV.3.2. Catalyst characterization for wash-coating process

Three different characterization techniques were employed to analyze the effect of catalyst impregnation on the open cell foams via spin-coating technique. Previously, the catalysts in powder form were analyzed by conventional characterization (Helium picnometry, H₂-TPR, CO₂-TPD, textural properties, etc).

1. The average thickness of the calcined coated structures was characterized by scanning electron microscopy instrument (Philips CM12 instrument).

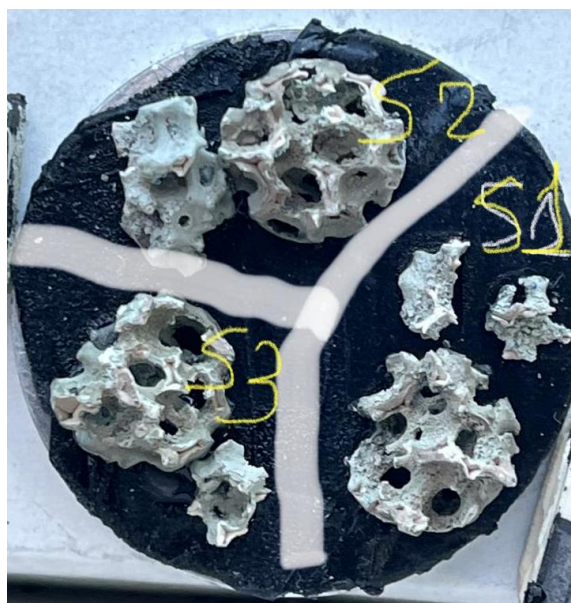


Figure IV- 5. Structured catalyst preparation for SEM characterization

2. Weight loss after sonication of the multiple flash-dried steps and the final calcined coated foam was studied by ultrasonic vibrations during 30 min with a mixture of petroleum ether and water. The weight of the structure was measured before and after sonication for calculation of the weight loss.
3. The rheological properties of the catalytic powder slurry were measured using a dynamic stress rheometer (Anton-Paar, MCR 92 model). Viscosity was recorded from 0.1 to 3000 s^{-1} shear rate range at 293 K. Additional information for shear stress (Pa) respect shear rate (s^{-1}) to obtain the yield point, τ ; and the storage modulus G' (Pa) and Loss Modulus G'' (Pa) respect shear Stress to analyze the representative shear stress fixing at an angular frequency of 10 rad/s was analyzed by this Anton-Paar model.

IV.4. Activity test for CO₂ methanation (Photo and Fixed bed reactor)

IV.4.1. Photo-reactor

Activity tests were performed in a bench-scale plant provided by (PID Eng&Tech) using a commercial photoreactor as shown in Figure IV- 6 A-B.

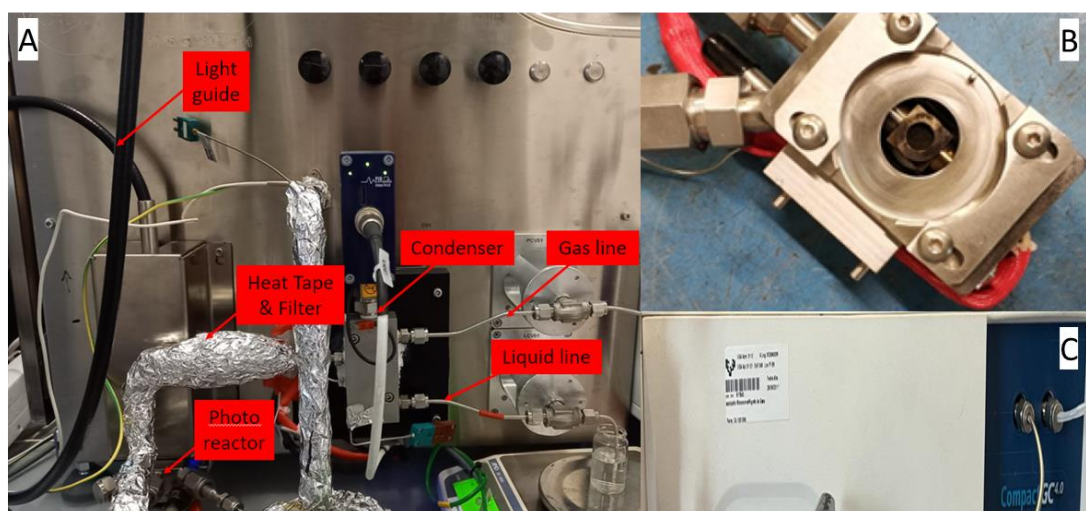


Figure IV- 6. A) Photoreactor PID plant. B) Raman High Temperature Reaction Chamber. C) Compact GC 4.0

For all tests, 25 mg of catalyst was loaded corresponding to a weight hourly space velocity (WHSV) of 53.5 h^{-1} at 9 bars. The reaction is performed in a photoreactor with an 8 mm open removable quartz window. The bench-scale plant (*PID Eng&Tech*) has two LED light source attached to the window for three different catalytic conditions: dark, UV (LED 365 nm) and visible (LED 470 nm). The composition of the effluent gases was analyzed by an online *CompactGC 4.0* gas chromatograph with a TCD and a flame ionization detector (FID). LED light intensity was analyzed by a *GL Optic Spectis 1.0* spectrometer coupled with an *Opti Sphere 48*.

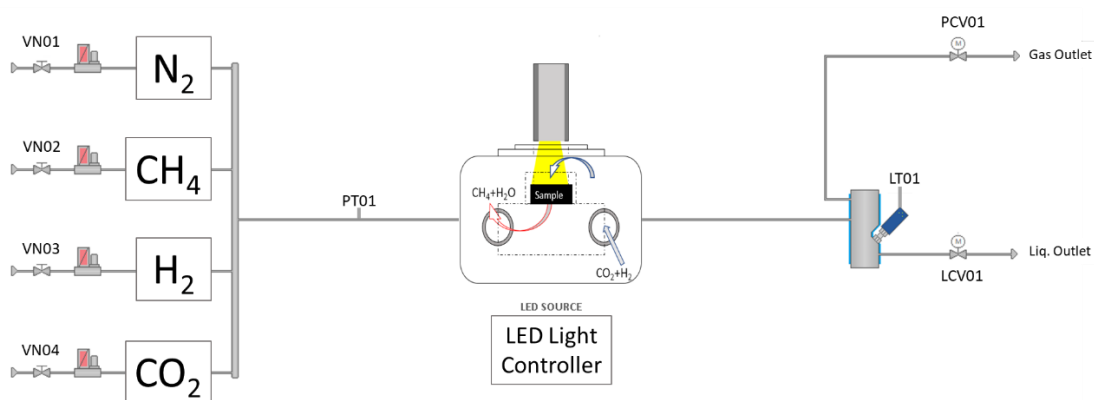


Figure IV- 7. Scheme of the photoreactor system

Monometallic $\text{Ni}/\text{Al}_2\text{O}_3$ and $13\text{Ni}/\text{TiO}_2$ catalysts were reduced in situ before the experimental tests at 723 K and 623 K respectively during 1.5 hours using a mixture of H_2 and N_2 in a 1:3 ratio. Monometallic Au/TiO_2 were in-situ reduced by sodium citrate during the synthesis process as discussed in catalyst preparation. For hydrotalcite materials, all samples were reduced ex-situ in a furnace depending on the H_2 -TPR peaks as it discussed in the results chapter. During the reaction step H_2 and CO_2 were fed gradually 2:1 (5 min) -3:1 (5 min) until 4:1 stoichiometry ratio with a total flow of

50 mL_N/min. The activity was analyzed in different temperature steps of 50 K from 473 to 723 K.

For the best catalytic activity results, the catalysts were tested for 16 h with the best photocatalytic conditions in order to study the possible deactivation of the catalysts.

The measured parameter analyzed were the following ones:

- Carbon dioxide conversion: $X_{\text{CO}_2} (\%) = (V_{\text{CO}_2}^{\text{in}} - V_{\text{CO}_2}^{\text{out}}) / V_{\text{CO}_2}^{\text{in}} \cdot 100$
- Hydrogen conversion: $X_{\text{H}_2} (\%) = (V_{\text{H}_2}^{\text{in}} - V_{\text{H}_2}^{\text{out}}) / V_{\text{H}_2}^{\text{in}} \cdot 100$
- Methane yield: $\text{CH}_4 \text{ yield } (\%) = V_{\text{CH}_4}^{\text{out}} / V_{\text{CO}_2}^{\text{in}} \cdot 100$
- $(\text{CH}_4/\text{H}_2\text{O})_{\text{out}}$ molar ratio: $(\text{CH}_4/\text{H}_2\text{O})_{\text{out}} = (V_{\text{CH}_4} / V_{\text{H}_2\text{O}})_{\text{out}}$

IV.4.2. Fixed-bed reactor

Structured catalysts were tested by a quartz fixed bed reactor keeping unchanged the volume of the material (diameter and length of 1 cm and 1.5 cm respectively). Before conducting catalytic tests, structured catalysts were reduced in-situ at 973 K. The reduction was carried out by exposing the catalyst to a flow of H₂/N₂ gas mixture with a composition of 50% hydrogen and 50% nitrogen. The flow rate of this gas mixture was set at 30 Nml·min⁻¹, and the temperature during this reduction process was maintained at 973°C for 1 hour. The reaction temperature was set from 573 K to 773 K varying the space velocity (GHSV = 10,000- 20,000 and 30,000 h⁻¹), the catalyst load (0.1- 0.2- 0.3 g/cm³) and foam PPI (20- 30- 40). To analyze the composition of both the reactants and the products, an on-line gas chromatograph (Agilent 6890 Plus) was employed. This chromatograph was equipped with thermal conductivity (TCD) and flame ionization (FID) detectors. TCD is commonly used to detect gases that have different thermal

conductivities, while FID is used for detecting hydrocarbons and other flammable substances. The measured parameter analyzed were the same as II.1.1.

References

- [1] Méndez-Mateos D, Barrio VL, Requies JM, Cambra JF. A study of deactivation by H₂S and regeneration of a Ni catalyst supported on Al₂O₃, during methanation of CO₂. Effect of the promoters Co, Cr, Fe and Mo. *RSC Adv* 2020;10:16551–64. <https://doi.org/10.1039/d0ra00882f>.
- [2] Ojea-Jiménez I, Campanera JM. Molecular modeling of the reduction mechanism in the citrate-mediated synthesis of gold nanoparticles. *J Phys Chem C* 2012;116:23682–91. <https://doi.org/10.1021/jp305830p>.
- [3] Chen J, Zhang J, Ye M, Rao Z, Tian T, Shu L, et al. Flexible TiO₂/Au thin films with greatly enhanced photocurrents for photoelectrochemical water splitting. *J Alloys Compd* 2020;815:152471. <https://doi.org/10.1016/j.jallcom.2019.152471>.
- [4] Chen WT, Chan A, Sun-Waterhouse D, Moriga T, Idriss H, Waterhouse GIN. Ni/TiO₂: A promising low-cost photocatalytic system for solar H₂ production from ethanol-water mixtures. *J Catal* 2015;326:43–53. <https://doi.org/10.1016/j.jcat.2015.03.008>.
- [5] Guerrero-Urbaneja P, García-Sancho C, Moreno-Tost R, Mérida-Robles J, Santamaría-González J, Jiménez-López A, et al. Glycerol valorization by etherification to polyglycerols by using metal oxides derived from MgFe hydrotalcites. *Appl Catal A Gen* 2014;470:199–207. <https://doi.org/10.1016/j.apcata.2013.10.051>.
- [6] Balzarotti R, Drago Ferrante G, Italiano C, Laganà M, Francis LF, Vita A, et al. RhNi/CeO₂ catalytic activation of alumina open cell foams by dip-spin coating

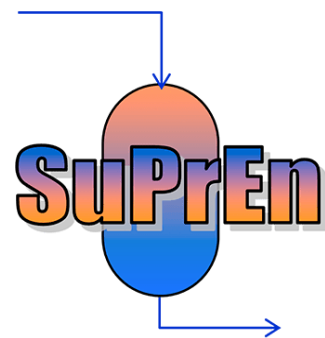
for the CO₂ methanation of biogas. *Surf Coatings Technol* 2022;441.
<https://doi.org/10.1016/j.surfcoat.2022.128563>.

- [7] Zhu Y, Lv G, Song C, Li B, Zhu Y, Liu Y, et al. Optimization of the washcoat slurry for hydrotalcite-based Int catalyst. *Catalysts* 2019;9.
<https://doi.org/10.3390/CATAL9080696>.



CHAPTER V

RESULTS AND DISCUSSION



Rafael Canales Larrazabal
Bilbao, 2023



Universidad
del País Vasco

Euskal Herriko
Unibertsitatea



Master eta Doktorego Eskola
Escuela de Máster y Doctorado
Master and Doctoral School

From articles:

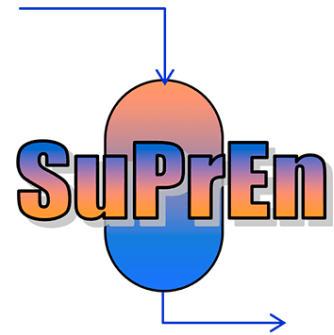
- UV- and visible-light photocatalysis using Ni–Co bimetallic and monometallic hydrotalcite-like materials for enhanced CO₂ methanation in Sabatier reaction. Authors: Rafael Canales, Miryam Gil-Calvo y V. Laura Barrio. Journal: Heliyon. DOI: <https://doi.org/10.1016/j.heliyon.2023.e18456>
- Photo- and Thermocatalytic CO₂ Methanation: A Comparison of Ni/Al₂O₃ and Ni–Ce Hydrotalcite-Derived Materials under UV and Visible Light. Authors: Rafael Canales y V. Laura Barrio. Journal: MDPI Materials. DOI: <https://doi.org/10.3390/ma16175907>
- Ni–Fe nanoparticles prepared using hydrotalcite precursors enhance the photocatalytic performance of CO₂ methanation. Authors: Rafael Canales, Ion Agirre and V. Laura Barrio. Journal: International Journal of Hydrogen Energy. Status: Accepted 11/12/2023

**El capítulo 5 está sujeto a confidencialidad
por el autor**



CHAPTER VI

CONCLUSIONS



Rafael Canales Larrazabal
Bilbao, 2023



Universidad
del País Vasco

Euskal Herriko
Unibertsitatea



Master eta Doktorego Eskola
Escuela de Máster y Doctorado
Master and Doctoral School

CHAPTER VI. CONCLUSIONS

In the current PhD thesis, an exhaustive study of different catalytic systems for the carbon dioxide methanation has been carried out. In addition to the conventional technologies already studied in previous theses, new knowledge of photocatalytic phenomena was added. Finally, the scaling up of the catalysts from lab scale to pilot plants was studied in order to be able to scale-up the catalytic systems to demo scale. Initially, knowing the optimal pressure conditions from previous projects, the optimal space velocity conditions for the reaction were calculated.

1. As an initial objective in the project, the preparation and analysis of catalysts with **Au** as an active noble metal and **TiO₂** as a support was done due to the high interest in photocatalysis and its high range of light absorption through the heterojunction effect, it was observed that it did not possess significant activity despite analyzing different synthesis methods and different **Au loadings**.
2. Comparing the thermo and photocatalytic activity of the **γ-Al₂O₃** and **P25 TiO₂** supports, it was concluded that the physico-chemical properties of alumina outperformed the photocatalytic improvements of titania. Comparing the thermo-photocatalytic activity of the Al₂O₃ and TiO₂ supports, it was concluded that the physico-chemical properties of alumina improved the photocatalytic enhancements due to the heterojunction effects of titania, improving the charge carry separation processes and the photonic adsorption enhancement.
3. Comparing the variation of alumina-impregnated nickel, **25%** was established as the optimum loading for higher thermo-photocatalytic activity. Under this nickel metal loading it was concluded that the method of preparing hydrotalcite derived

materials with nickel due to its higher CO₂ adsorption improved the results with respect to the monometallic alumina method.

Hydrotalcites were synthesized with different metal replacements: aluminum by ceria, cobalt by nickel and iron by aluminum.

4. The partial replacement of **Al by Ce** on the structure enhanced the activity at lower temperatures because the oxygen vacancies and the defects provided by CeO₂ improved the adsorption of CO₂ and the catalytic activity. The mixed oxide with a Ce/Al molar atomic ratio of 0.22 had improved photocatalytic activity at lower temperatures, achieving 50% CO₂ conversion, 46% CH₄ yield, and almost 99.5% CH₄ selectivity under visible light at **473 K**.
5. Comparing the hydrotalcites partial replacement of **Co by Ni** as active centre, the best results were achieved under visible light for the 6Co-21Ni and 27Ni catalysts, where a CO₂ conversion of 73% was observed at 528 K with a slightly higher conversion for the 27Ni catalyst. Thus, the Co addition did not improve the methanation performance due to the CoO species involved in the reaction which were not active for Sabatier process but active for reverse water gas shift. The reduction of spinel CO₃O₄ to Co⁰ did not improve the previous Ni⁰ activity results due to its complex reducibility.
6. For the Fe-based content catalysts, partial replacement **Al by Fe** of them presented strong absorbance in the UV-visible region, narrowing the band gap, but photocatalytic CO₂ conversion is not enhanced due to the presence of iron and nickel species with lower reduction temperature. Thus, the slightly higher Mg content as a consequence of this molar substitution increased the formation of

moderately strong basic sites, which may be responsible for the higher methanation activity at 523 K.

7. For the Mo-based content catalysts, the impregnation with Mo did not improve the activity with respect to the monometallic one. The low reducibility to metallic Mo and probably its deposition on active nickel centers worsened the results in all catalytic and photocatalytic conditions.

With regard to the study during the collaboration between UPV/EHU and the CNR-ITAE, it was concluded that in order to impregnate catalysts on the alumina open cell foams the variation of the contents in the aqueous solution such as PVA, glycerol and water affected the adhesion of the catalyst on the alumina and its thickness. The best wash-coating preparation process according to the results in terms of mechanical stability, average thickness and pore per inch (PPI) were as follows:

1. 2000 rpm for 20 s during dip/spin-coating procedure.
2. A slurry preparation solution of PVA/(Water + Glycerol)= 2.0% and Water/Catalyst=1.5% was fixed as the optimal procedure content.
3. 30 PPI alumina open cell foam was selected as the best structured material due to lower catalytic loss during sonication treatment.
4. Mathematical models can be used for the determination of coating thickness impregnation.
5. Lower thermal gradient and less pressure drop can be overcome with structured catalysts.

INDEX OF FIGURES AND TABLES

CHAPTER I

Figure I-1. Fuel mix in Gross Inland Consumption in Europe.....	4
Figure I-2. Global CO ₂ emissions from energy combustion and industrial processes, 1900-2022 [2].....	5
Figure I-3. Renewable annual net capacity additions by technology, main and accelerated cases, 2015-2027 [3].....	6
Figure I-4. Global methane emissions from the energy sector over time, 2000-2021 [6].....	8
Figure I-5. Biogas production by region and by feedstock type [9].....	9
Figure I-6. 17 Image of the 17 Sustainable Development Goals.	10

CHAPTER II

Figure II- 1. Power-to-Fuel scheme.....	18
Figure II- 2. Existing Power-to-Gas Projects Worldwide as of September 2019. Source: Technical University of Applied Sciences (OTH)/POWER magazine.	19
Figure II- 3. Battery electric and fuel-cell electric vehicle (BMW X5 prototype).....	22
Figure II- 4. Type of water electrolyzers.....	23
Figure II- 5. Selected synthesis pathways for H ₂ +CO ₂ [24].....	29
Figure II- 6. Scheme of a fixed bed reactor for CO ₂ methanation [27].	30
Figure II- 7. A) Fixed bed reactor used in the CNR-ITAE. B) Commercial catalyst impregnated on alumina open cell foam.....	31
Figure II- 8. Fluidized bed reactor for CO ₂ methanation on the Gaya platform [28].	32
Figure II- 9. Scheme of a three-phase reactor for CO ₂ methanation [29].	32
Figure II- 10. Harrick commercial photoreactor	34

Figure II- 11. Standard solar spectra for space and terrestrial use.	34
Figure II- 12. A) Charge transfer mechanism; B) local electric field enhancement mechanism [32].....	36
Figure II- 13. Results of the 2023 EU criticality assessment [34]	38
Figure II- 14. Scheme of the structure of the hydrotalcite	41
Table II- 1. CRMs used during the thesis	37
Table II- 2. Summary of various CO ₂ methanation catalysts and photocatalysts.....	43
CHAPTER IV	
Figure IV- 1. Hydrotalcite structural changes during synthesis and calcination process.	68
Figure IV- 2. Summary of wash-coating procedure and image.....	74
Figure IV- 3. Left) Rheological properties analyzer. Right) Spin-coater equipment.....	76
Figure IV- 4. Slurry after ball-milling and sonication. Left: Ce-Hydrotalcite. Right: Katalco.....	76
Figure IV- 5. Structured catalyst preparation for SEM characterization	77
Figure IV- 6. A) Photoreactor PID plant. B) Raman High Temperature Reaction Chamber. C) Compact GC 4.0.....	78
Figure IV- 7. Scheme of the photoreactor system	79
Table IV- 1. The nominal content of the HTC-Ce.....	69
Table IV- 2. The nominal content of the HTC-Co.....	69
Table IV- 3. The nominal content of the HTC-Fe	69
Table IV- 4. The nominal content of the HTC-Mo	70
Table IV- 5. Characteristics of the open cell foams used	75

CHAPTER V

Figure V- 1. H ₂ -TPR results of 13Ni/Al ₂ O ₃ , 25Ni/Al ₂ O ₃ and 13Ni/TiO ₂	90
Figure V- 2. CO ₂ -TPD results of 13Ni/Al ₂ O ₃ , 25Ni/Al ₂ O ₃ and 13Ni/TiO ₂	91
Figure V- 3. Diffuse reflectance UV-vis spectra of monometallic catalysts.	92
Figure V- 4. STEM images of monometallic nickel catalysts	93
Figure V- 5. Activity comparison: A) Dark reaction. B) UV (365 nm). C) Visible (470 nm)	94
Figure V- 6. H ₂ -TPR profiles of the calcined catalysts.....	97
Figure V- 7.CO ₂ -TPD profiles of (A) calcined HTCs and (B) Ni/Al ₂ O ₃ catalysts.	99
Figure V- 8. XRD profiles of hydrotalcites: (A) dehydrated; (B) reduced. (C) Comparison of the crystallinity of 25Ni/Al ₂ O ₃	101
Figure V- 9. Comparison of the XPS spectra: (A) reduced Ni 2p, (B) used Ni 2p (D), (C) reduced O 1s, and (D) reduced Ce 3d.....	104
Figure V- 10. Diffuse reflectance UV–vis spectra of (A) hydrotalcite and (B) monometallic catalysts.....	106
Figure V- 11.Comparison of activity enhanced by temperature dark (A), UV light (B), and visible light (C). Stability of HTC 4 under visible light for 24 h at 523 K (D).	107
Figure V- 12. Scanning transmission electron microscopy (STEM) images of the used catalysts and the particle size frequency and energy dispersive X-ray spectroscopy (EDS) for the analysis of the surface dispersion of metal.....	113
Figure V- 13. XRD patterns of: a) dried catalysts and b) calcined catalysts at 773 K.....	116
Figure V- 14. Reduction profiles for calcined hydrotalcite-derived materials.....	117
Figure V- 15. CO ₂ -TPD profiles of the calcined hydrotalcite-derived materials.	118
Figure V- 16. a) UV-vis DRS spectra of calcined samples and b) direct band gap obtained from K-M absorbance spectra.	120

Figure V- 17. XPS spectra of the reduced hydrotalcite-derived catalysts a) Co 2p _{3/2} and 2p _{1/2} and b) Ni 2p _{3/2} . and 2p _{1/2}	121
Figure V- 18 .STEM-EDS images of ²⁷ Co, ¹⁹ Co-8Ni, 6Co-21Ni, and ²⁷ Ni catalysts.....	122
Figure V- 19. CO ₂ conversion and CH ₄ yields under thermal conditions.....	123
Figure V- 20 .CO ₂ conversion and CH ₄ yields under UV light irradiation.	124
Figure V- 21. CO ₂ conversion and CH ₄ yields under visible-light irradiation.	125
Figure V- 22. Photocatalytic stability tests for ²⁷ Ni and 6Co-21Ni catalysts in CO ₂ methanation at 523 K.	125
Figure V- 23. XRD patterns for the catalysts: A) Non-calcined hydrotalcites, B) calcined hydrotalcite materials, C) 25Ni/Al ₂ O ₃ in the reduced state and used under dark and UV photocatalytic experiments.	128
Figure V- 24. H ₂ -TPR deconvolution profiles of the calcined catalysts.	129
Figure V- 25.XPS deconvolution: A) Ni 2p _{3/2} and B) Fe 2p _{3/2}	131
Figure V- 26. A) UV–vis DR spectra of the catalysts; B) Optical direct band gaps.	133
Figure V- 27. CO ₂ -TPD profile representation of the reduced catalysts.	135
Figure V- 28. General STEM-HAADF images, EDS mapping for Ni-Fe NPs and particle size analysis.....	136
Figure V- 29. Temperature-dependent CO ₂ conversion & CH ₄ yield measured under various illumination conditions: A-B) dark; C-D) UV; E-F) visible.	137
Figure V- 30. A) CO ₂ conversion using 25Ni/Al ₂ O ₃ and 25Ni-HTC under visible photocatalytic conditions at 523 K. B) Summary of the relationship between band gap and CO ₂ conversion under different light conditions. C) Enhancement of the CO ₂ conversion under UV & visible light compared to dark conditions at 523 K.....	141
Figure V- 31. H ₂ -TPR and CO ₂ -TPD profiles of Mo promoter catalysts	143
Figure V- 32. Mo ₂ -HTC Catalytic tests.....	144
Figure V- 33. Mo ₃ -HTC Catalytic tests.....	144

Figure V- 34. Left) Rheological properties of Katalco. Viscosity vs Shear rate. Right) Weight loss after sonication treatment	145
Figure V- 35. Thermogravimetric analysis curves of weight loss associated with liquid evaporation during flash drying and calcination process. The slurry TGA corresponded to the commercial catalyst (5g) with same liquid composition.....	147
Figure V- 36. Coating loading depending on spinning velocity.....	147
Figure V- 37. Average thickness at 500-1000-2000 rpm	148
Figure V- 38. Number of washcoating deposition vs catalyst load on alumina foam.....	149
Figure V- 39. Weight loss depending on the catalyst coated. Average thickness of 0.2 and 0.3 g/cm ³ ...	149
Figure V- 40. Influence of PPI on wash-coating thickness fixing coating load	150
Figure V- 41. Weight loss after sonication of 20, 30 and 40 PPI alumina foam	150
Figure V- 42. Influence of compound modification for slurry preparation. A) Different PVA products. B) Variation of water content (5-7.5-10-12 ml). C) Variation of glycerol content.	152
Figure V- 43. Viscosity estimation as function of surface area and powder density.....	152
Figure V- 44. Slurry Shrinkage due to thermal treatment	153
Figure V- 45. Yield point and Rep. Shear Stress calculation.....	155
Figure V- 46. Influence of RPM variation and g/cm ³ wash-coating load on layer thickness.....	156
Figure V- 47. Activity comparison with 30 PPI alumina open cell foam varying GHSV and g/cm ³	158
Figure V- 48 .Temperature gradient at different positions and activity conditions.	159
Figure V- 49. Activity comparison varying PPI open cell foam.....	159
Table V- 1. Textural properties and metal composition.....	89
Table V- 2. CO ₂ -TPD profiles of monometallic catalysts	91
Table V- 3. H ₂ -Chemisorption of monometallic catalysts	93

Table V- 4. Summary of the metal contents and the textural properties	96
Table V- 5. Basic sites for the calcined catalysts	99
Table V- 6. Crystal size of the non-calcined HTCs.....	100
Table V- 7. Results of H ₂ chemisorption.....	102
Table V- 8. Metal/Al atomic ratios obtained from the XPS results of the reduced and calcined catalysts.	103
Table V- 9. (A) Difference in CO ₂ conversion between dark and UV-irradiated conditions. (B) Comparison of activity in the dark vs. under visible light.....	110
Table V- 10. Elemental composition obtained from ICP-OES and textural properties	114
Table V- 11. Basic sites for the calcined hydrotalcite-like materials (HTCs)	118
Table V- 12. Summary of the catalysts's metal loading and textural properties.....	126
Table V- 13. XPS spectra results for the reduced samples.....	132
Table V- 14. Proportions of basic sites and distribution.....	134

PERSONAL DATA

- Name and surname: **Rafael Canales Larrazabal**
- Date of birth: June 5, 1993.
- Address: C/ Urquijo 2, 3^ºIzq (Las Arenas-Getxo) Bizkaia
- Telephone number: +34 628 868 155
- email: rafael.canales@ehu.eus



ACADEMIC INFORMATION

- Degree in Environmental Engineering at the *School of Engineering of Bilbao (UPV/EHU)*
- Master's degree in Sustainable Energetical Engineering at the *School of Engineering of Bilbao (UPV/EHU)*
- PhD student at the School of Engineering of Bilbao (UPV/EHU) in the SuPrEn research group under the project: *Advanced Catalytic and Photocatalytic Technologies for Methane Generation from Renewable Energies.*
- Four-month-research stay at the *Istituto di Tecnologie Avanzate per l'Energia-CNR (CNR-ITAE)-Messina.*

LANGUAGES

- Español (Native)
- Inglés (High level)
- Euskera (Medium level)

SOFTWARE

- Microsoft Office (Word, Excel, Access, Project...), Internet, Auto Cad, Solid Edge
- Matlab/Simulink
- Aspen Plus
- Epanet y Storm Water Management Model (SWMM)
- Pyrosim

CONFERENCE ATTENDANCE

- FOTOFUEL Workshop on Solar Fuels, IMDEA energía Móstoles (Madrid), 2019.
- 12TH International Conference on Hydrogen Production (ICH2P) 2021. Oral Presentation: Study of photo and thermocatalytic CO₂ methanation on Ni/Al₂O₃ and hydrotalcite-like catalysts.
- European Hydrogen Energy Conference (EHEC) 2022. Oral Presentation: Activity of bi-metallic hydrotalcite derived materials for photocatalytic CO₂ methanation.
- HYCELTEC 2022 VIII Symposium on Hydrogen, Fuel Cells and Advanced Batteries. Oral Presentation: Preparation of Ni-Fe alloys from hydrotalcite precursors for carbon dioxide methanation.
- 2nd Renewable Hydrogen Energy Conference (RH2EC) 2023. Oral Presentation: Wash-coating of Ni based systems on alumina open cell foam for CO₂ methanation.

PUBLICATIONS

- UV- and visible-light photocatalysis using Ni–Co bimetallic and monometallic hydrotalcite-like materials for enhanced CO₂ methanation in Sabatier reaction. Authors: Rafael Canales, Miryam Gil-Calvo y V. Laura Barrio. Journal: Heliyon. DOI: <https://doi.org/10.1016/j.heliyon.2023.e18456>
- Photo- and Thermocatalytic CO₂ Methanation: A Comparison of Ni/Al₂O₃ and Ni–Ce Hydrotalcite-Derived Materials under UV and Visible Light. Authors: Rafael Canales y V. Laura Barrio. Journal: MDPI Materials. DOI: <https://doi.org/10.3390/ma16175907>
- Ni–Fe nanoparticles prepared using hydrotalcite precursors enhance the photocatalytic performance of CO₂ methanation. Authors: Rafael Canales, Ion Agirre and V. Laura Barrio. Journal: International Journal of Hydrogen Energy. Status: Accepted.